

General Protein Pretraining or Domain-Specific Designs? Benchmarking Protein Modeling on Realistic Applications

Shuo Yan^{1,*}, Yuliang Yan^{1,*}, Bin Ma¹, Chenao Li¹, Haochun Tang¹

Jiahua Lu¹, Minhua Lin², Yuyuan Feng³, Enyan Dai^{1,†}

¹Hong Kong University of Science and Technology (Guangzhou)

²The Pennsylvania State University

³Xiamen University

Abstract

Recently, extensive deep learning architectures and pretraining strategies have been explored to support downstream protein applications. Additionally, domain-specific models incorporating biological knowledge have been developed to enhance performance in specialized tasks. In this work, we introduce **Protap**, a comprehensive benchmark that systematically compares backbone architectures, pretraining strategies, and domain-specific models across diverse and realistic downstream protein applications. Specifically, Protap covers five applications: two general tasks and three novel specialized tasks, i.e., enzyme-catalyzed protein cleavage site prediction and targeted protein degradation, which are industrially relevant yet missing from existing benchmarks. For each application, Protap compares various domain-specific models and general architectures under multiple pretraining settings. Our empirical studies imply that: (i) Though large-scale pretraining encoders achieve great results, they often underperform supervised encoders trained on small downstream training sets. (ii) Incorporating structural information during downstream fine-tuning can match or even outperform protein language models pretrained on large-scale sequence corpora. (iii) Domain-specific biological priors can enhance performance on specialized downstream tasks. Code is publicly available at <https://github.com/Trust-App-AI-Lab/protap>.

1 Introduction

Proteins serve as the central executors of biological activities, regulating a wide range of critical biological processes through their complex three-dimensional structures and dynamic properties. A precise understanding of protein function and interactions is critical across many applications [2, 65]. For instance, directed evolution of enzymes can endow proteins with novel functions [4]. Accurate prediction of protein–ligand interactions (PLIs) can largely accelerate drug discovery [55, 66, 72]. These application areas underscore the immense potential of deep learning in protein analysis.

Various deep model architectures and pretraining tasks have been developed to leverage protein sequences and structures for protein applications. (i) *General Architectures*: Sequence models such

as LSTM [23] and Transformer [63] have been employed to extract amino acid sequence patterns for tasks like stability landscape prediction [50]. Geometric Graph Neural Networks (GNNs), including GVP-GNN [27] and EGNN [56], have demonstrated remarkable effectiveness in modeling 3D protein structures [11, 41]. Recently, Graphformer [71] and Transformer-M [36] further incorporated structural biases into transformer-based architectures. These emerging sequence-structure hybrid models show promising ability in protein representation learning. (ii) *Pretraining Strategies*: Recently, large-scale protein pretraining models have also been explored to benefit the representation learning for downstream applications. In particular, masked language modeling has been extended to predict the masked amino acids in protein sequences, resulting in protein language models like ESM and ProteinBERT [6, 21, 54]. Moreover, GearNet [74] explores the multi-view contrastive learning on protein structures. Additionally, some methods, such as OntoProtein [73], leverage functional annotations as supervision signals for protein encoder pretraining.

Apart from these neural architectures and pretraining tasks for protein modeling, significant progress has also been made in developing domain-specific models for various downstream protein applications. For instance, protein function prediction models such as DPFunc [64] leverage sequence, structural, and domain-level information to enhance the accuracy of predicting the Gene Ontology annotations of proteins. Additionally, to improve enzyme modeling, UniZyme [31] integrates the energy frustration matrix and enzyme active-site knowledge into a transformer-based framework. In the domain of proteolysis-targeting chimera (PROTAC) modeling, dedicated methods such as DeepProtacs [32] and ETProtacs [8] have been developed to accurately capture the ternary interactions essential for targeted protein degradation.

Given the extensive variety of general model architectures, pretraining strategies, and domain-specific models, there remains a gap in benchmarking general pretrained models alongside domain-specific models. This leads us to a fundamental question: *Can large-scale general pretrained models outperform domain-specific models on downstream protein tasks? If so, under what conditions, and which model architectures or pretraining strategies enable such advantages?* However, current benchmarks predominantly focus on specific pretrained model categories, such as protein language models in [9, 68] and geometric GNNs in [26]. The comparisons of our Protap with existing benchmarks are given in Appendix Tab. 5. In summary, existing works lack a comprehensive evaluation of general protein model architectures, pretraining strategies, and domain-specific models across realistic biological applications. To address these

Permission to make digital or hard copies of all or part of this work for personal or classroom use is granted without fee provided that copies are not made or distributed for profit or commercial advantage and that copies bear this notice and the full citation on the first page. Copyrights for components of this work owned by others than the author(s) must be honored. Abstracting with credit is permitted. To copy otherwise, or republish, to post on servers or to redistribute to lists, requires prior specific permission and/or a fee. Request permissions from permissions@acm.org.

Preprint,

© 2026 Copyright held by the owner/author(s). Publication rights licensed to ACM.
ACM ISBN 978-1-4503-XXXX-X/26/08
<https://doi.org/XXXXXXXX.XXXXXXX>

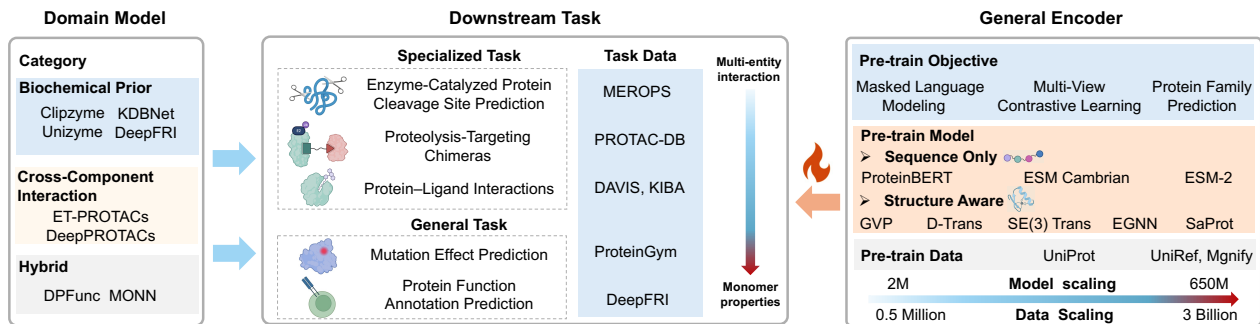


Figure 1: Overview of our benchmark Protap.

gaps, we introduce Protap, a standardized benchmark that compares architectures, pre-training strategies, and domain models on five realistic downstream applications. Our contributions are:

- We identify and integrate realistic applications from existing literature and databases to support comprehensive evaluations. In addition to two general applications, Protap introduces two novel specialized applications: enzyme-catalyzed protein cleavage site prediction and targeted protein degradation by PROTACs, which are biological processes not covered by prior benchmarks. Furthermore, Protein-Ligand Interaction is also categorized as a specialized application due to its complex molecular interactions.
- Comprehensive and diverse proteins are covered in the benchmark, which include enzymes, receptors, drugs, etc. The tasks are diverse, which include single protein modeling, interaction modeling such as PLI, enzyme-substrate modeling, and complex interaction process modeling, i.e., PROTACs.
- We compare 18 protein pretraining models and 8 domain models across 5 realistic protein applications. This offers insights into the development of protein foundation models and the design of domain-specific models for downstream applications.

2 Related Works

Existing benchmarks for protein modeling primarily emphasize sequence-based models. TAPE [50] introduces standardized sequence-centric tasks, including structure prediction and remote homology detection. PEER [68] expands the sequence-based scope to cover protein-protein interactions and functional annotations. ProteinGLUE [9] is another sequence-based benchmark designed to evaluate sequence pretraining methods. ProteinGym [47] establishes an evaluation framework for mutation effect prediction with protein language models. ProteinBench [70] evaluates protein foundation models mainly in protein generation tasks. Among existing benchmarks, ProteinWorkshop [26] incorporates the equivariant graph neural networks to evaluate the structure-based models. However, ProteinWorkshop lacks a unified benchmarking pipeline that systematically compares sequence-based, structure-based, and hybrid models within a standardized framework.

Furthermore, existing benchmarks predominantly focus on general model architectures such as LSTMs [23], Transformers [63], and EGNNs [56]. In contrast, Protap explores the advantages of domain-specific model designs and the integration of domain knowledge. Our Protap systematically benchmarks domain-specific models

alongside pretrained models with general architectures. This can provide deeper insights into effective model design and performance. Moreover, Protap introduces two novel specialized applications: enzyme-catalyzed protein cleavage site prediction and targeted protein degradation by PROTACs, which are biological processes not considered by prior benchmarks. A more comprehensive comparison between existing benchmarks is presented in Tab. 5.

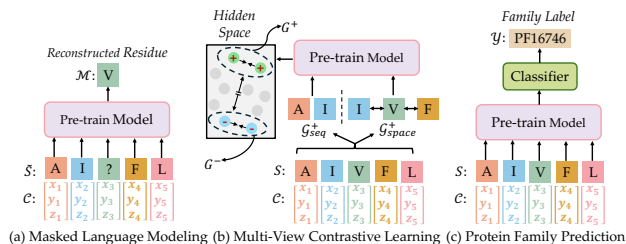


Figure 2: Illustration of pretraining tasks in Protap.

3 Protein Pretraining Models in Protap

In this section, we first outline the fundamental definitions of protein sequences and structures. We then introduce the three pretraining tasks employed in Protap: masked language modeling, multi-view contrastive learning, and protein family prediction. Finally, we summarize the protein pretraining models deployed in the Protap benchmark.

3.1 Preliminaries of Proteins

A protein is composed of an amino acid sequence that folds into 3D structures. We denote a protein with a residue sequence of length n by $\mathcal{P} = (\mathcal{S}, \mathcal{C})$, where \mathcal{S} is the set of sequential residues and \mathcal{C} denotes the spatial coordinates of residues. The structural information is represented as $\mathcal{C} = [c_1, c_2, \dots, c_n]$, where each c_i corresponds to the three-dimensional position of the $C\alpha$ atom of residue a_i . We adopt $C\alpha$ atoms as backbone anchors, as they provide a stable and widely used structural reference in protein modeling. More information about the sequence and structures of the proteins can be found in Appendix E.

3.2 Pretraining Tasks and Pretraining Models

Recently, the pretraining paradigm has achieved remarkable success across text, images, and graphs [1, 13, 24, 49]. To facilitate

Table 1: Overview of models and datasets used in Protap.

(a) Pretraining models and domain models in our Protap. Models highlighted in (*) are trained from scratch, while those in (†) use only publicly available pretrained weights.

Model	Input Modalities	Pretrain Data	#Parameter	Training Objective	Source
Pretrain Models					
EGNN	AA Seq & 3D Coord	Swiss-Prot 540k	10M	MLM, MVCL, PFP	ICML, 2021
SE(3) Transformer	AA Seq & 3D Coord	Swiss-Prot 540k	4M	MLM, MVCL, PFP	NeurIPS, 2020
GVP	AA Seq & 3D Coord	Swiss-Prot 540k	2M	MLM, MVCL, PFP	ICLR, 2021
ProteinBERT	AA Seq	Swiss-Prot 540k	72M	MLM, MVCL, PFP	Bioinformatics, 2022
D-Transformer	AA Seq & 3D Coord	Swiss-Prot 540k	3.5M	MLM, MVCL, PFP	NeurIPS, 2025, ICLR, 2023
ESM-2	AA Seq	UR50 70M	650M	MLM	Science, 2023
ESM Cambrian	AA Seq	UR70, MGnify, JGI 3B	600M	MLM	Science, 2025
SaProt	AA Seq & 3D Coord	UR50 40M	650M	MLM	ICLR, 2024
Domain Specific Models					
ClipZyme	AA Seq & 3D Coord & SMILES	–	14.8M	PCS	ICML, 2024
UniZyme	AA Seq & 3D Coord	Swiss-Prot 11k	15.5M	PCS	NeurIPS, 2025
DeepProtacs	AA Seq & 3D Coord & SMILES	–	0.1M	PROTACs	Nature Communications, 2022
ETProtacs	AA Seq & 3D Coord & SMILES	–	5.4M	PROTACs	Briefings in Bioinformatic, 2025
KDBNet	AA Seq & 3D Coord & SMILES	–	3.4M	PLI	Nature Machine Intelligence, 2023
MONN	AA Seq & 3D Coord	–	1.7M	PLI	Cell Systems, 2024
DeepFRI	AA Seq & 3D Coord	Pfam 10M	1.8M	PFA	Nature Communications, 2021
DPFunc	AA Seq & 3D Coord & Protein Domain	–	110M	PFA	Nature Communications, 2025

(b) Summary of datasets and metrics for various prediction tasks.

Application	Category	Data Source	#Train	#Test	Metric
Pretraining	–	[10]	542,378	–	–
Protein Cleavage Site Prediction	Specialized	[51]	1609	316	AUC, AUPR
Targeted Protein Degradation	Specialized	[19]	843	209	Acc, AUC
Protein–Ligand Interactions	Specialized	[37]	11,520	2,880	MSE, Pearson
Protein Function Annotation Prediction	General	[20, 26]	23,760	2,023	Fmax, AUPR
Mutation Effect Prediction	General	[47]	–	2.4M	AUC, Pearson

protein modeling, various pretraining strategies and model architectures have also been investigated [6, 35, 54, 58]. In this work, our Protap conducts a comprehensive analysis of representative protein pretraining tasks and models to systematically understand their capabilities and limitations in downstream applications. The models and pretraining tasks provided in Protap are summarized in Tab. 1 and briefly introduced below.

Pretraining Task 1: Masked Language Modeling (MLM).

This pretext task is based on the sequence information. A protein’s amino acid sequence adheres to an inherent grammar that encodes its structural and functional properties [2]. Therefore, inspired by the success of text modeling, masked language modeling has been adopted to train the protein language model [54] to capture patterns underlying residue sequences. Specifically, as Fig. 2 (a) shows, MLM aims to fill in missing amino acids in protein sequences given the masked residue sequence of a protein. ProteinBERT [6], ESM2 [35], ESM Carbrain [21], and various other protein language models have been pretrained using this MLM task.

Pretraining Task 2: Multi-View Contrastive Learning (MVCL).

This pretext task is based on the structural information. Protein structure plays a vital role in determining its biological function.

Furthermore, the local structures (motifs) within a protein are biologically related [39, 48]. Inspired by this, multi-view contrastive learning (MVCL) has been extended to preserve the representation similarity between the correlated substructures of proteins [74]. As shown in Fig. 2 (b), given a protein \mathcal{P} , we generate two views \mathcal{G}_{seq}^+ and \mathcal{G}_{space}^+ from its amino acid sequence as positive samples. Views from unrelated proteins serve as negative samples. The MVCL objective is to align positive samples while contrasting them with negative samples in the hidden representation space.

Pretraining Task 3: Protein Family Prediction (PFP).

Different from the MLM and MVCL, this task leverages auxiliary protein knowledge to introduce functional and structural supervision into protein representation learning. A protein family is a group of evolutionarily related proteins descended from a common ancestor, typically sharing similar three-dimensional structures, functions, and significant sequence similarities [5, 57]. Consequently, the Protein Family Prediction (PFP) task has been widely utilized to learn structurally contextualized representations [43]. As illustrated in Fig. 2 (c), Protap also deploys the protein family prediction to predict the ground-truth family labels y given the sequence S and the associated coordinate C .

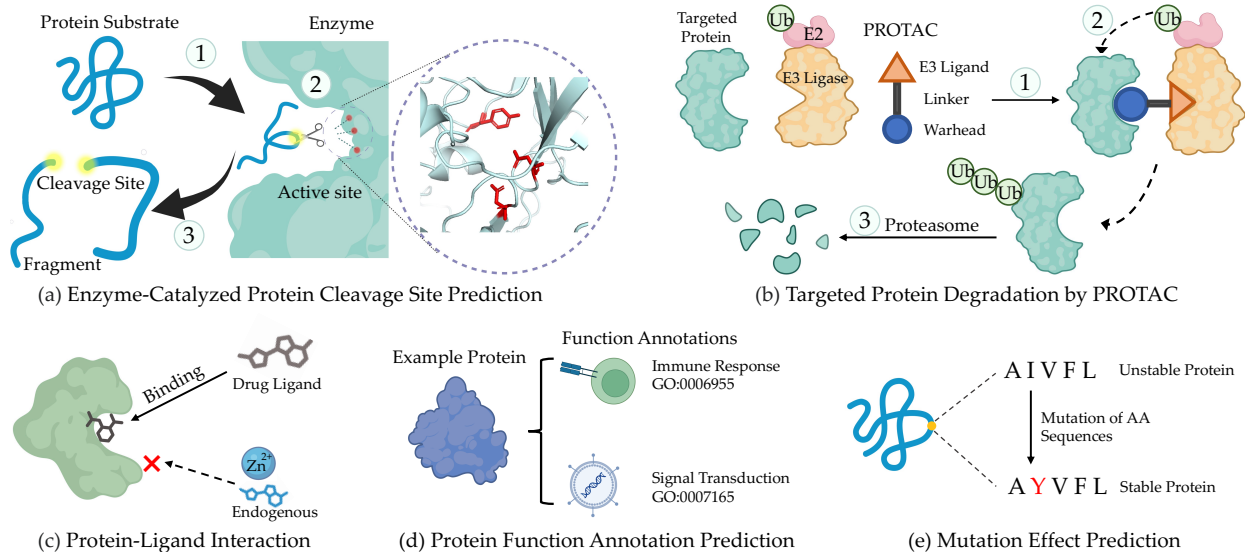


Figure 3: Illustration of downstream applications in Protap. (a) Biological process of the enzyme-catalyzed protein hydrolysis; (b) Biological process of targeted protein degradation by PROTACs, where PROTACs form a ternary complex with the target protein and E3 ligase, leading to target protein ubiquitination and degradation; (c) In protein-ligand interaction, the ligand binds to the protein pocket, blocking interactions with other molecules; (d) Protein function annotation prediction reveals the biological activities a protein participates in; (e) Mutation effect prediction optimizes protein properties or functions for protein engineering.

3.3 Pretraining Models

In Protap, we incorporate the following three categories of model architectures pretrained by the aforementioned pretext tasks:

- **Sequence-based model:** ProteinBERT [6], ESM-2 [35] and ESM Carbrain [21] treat the protein sequences as biological languages and adopt the transformer [63] to extract the sequential patterns.
- **Structure-based model:** Protap also implements EGNN [56], SE(3) transformer [17], and GVP [27], which are representative equivariant architectures for structural information encoding.
- **Sequence-structure hybrid model:** SaProt [58] enhances the protein language model with explicit structure vocabulary. Additionally, inspired by Transformer-M [36] and Unizyme [31], Protap implements a D-Transformer, which introduces the residue distance matrix into the sequence attention computation as shown in Tab. 1.

Protap pretrains ProteinBERT, EGNN, SE3 transformer, GVP, and D-Transformer on each pretraining task with UniProt [10], yielding 15 pretraining models. For the ESM-2, ESM-C and SaProt, we directly adopt their publicly available pretrained weights for protein modeling. More details of pretraining model architectures, pretraining datasets, and other pretraining details are given in Appendix G.

4 Applications and Domain Models

In this subsection, we introduce the applications adopted in Protap, categorized into specialized and general. Specialized applications focus on interaction or biological processes, which include Enzyme-Catalyzed Protein Cleavage Site Prediction, Targeted Protein Degradation by Proteolysis-Targeting Chimeras and Protein-Ligand Interactions. General applications broadly apply across diverse proteins,

which cover Protein Function Annotation Prediction and Mutation Effect Prediction for Protein Optimization. A complete list of implemented domain models is provided in Tab. 1, and detailed experimental setups including datasets and metrics are available in Appendix F.

Specialized Application 1: Enzyme-Catalyzed Protein Cleavage Site Prediction (PCS).

Application Description of PCS. As illustrated in Fig. 3, proteolytic enzymes will first recognize specific amino acid sequences or structural motifs within substrate proteins with the enzyme’s active sites. Then, the enzymes catalyze the cleavage of peptide bonds at the cleavage site. This fundamental biological process regulates protein activity, turnover, and signaling across diverse biological contexts. Predicting the protein cleavage sites under the catalysis of enzymes has many crucial applications, such as enzyme engineering and therapeutic target identification. For example, in the design of enzyme inhibitors or prodrugs, identifying key cleavage peptides under the catalysis of the HIV enzyme could enhance drug specificity [38]. The enzyme-catalyzed protein cleavage site prediction can be formulated as a residue-level binary classification task. Specifically, let \mathcal{P}^s and \mathcal{P}^e denote the protein substrate and enzyme. The protein cleavage site predictor aims to learn the following function:

$$f : (\mathcal{P}^s, \mathcal{P}^e) \rightarrow \{0, 1\}^{|\mathcal{P}^s|}. \quad (1)$$

PCS Domain Models. The majority of existing methods, such as Procleave [33], construct enzyme-specific features to identify the cleavage sites under the enzyme of interest. Recently, UniZyme [31]

has leveraged both enzyme and substrate encoders to build a unified cleavage site predictor that generalizes across various enzymes.

Specialized Application 2: Targeted Protein Degradation by Proteolysis-Targeting Chimeras (PROTACs).

Application Description of PROTAC. A Proteolysis-targeting chimeras (PROTAC) is a heterobifunctional molecule consisting of three components: a ligand for the targeted protein (commonly referred to as the warhead), a chemical linker, and a ligand that recruits an E3 ubiquitin ligase. PROTACs have emerged as powerful tools for selectively degrading disease-associated proteins via the ubiquitin-proteasome system [40]. As shown in Fig. 3, the PROTAC-mediated degradation process begins with simultaneous binding of the PROTAC to the target protein and an E3 ligase, resulting in a ternary complex. This complex subsequently facilitates the transfer of ubiquitin from the E2 enzyme to the target protein, ultimately leading to its proteasomal degradation. PROTACs offer several advantages over conventional treatments. First, due to their catalytic mode of action, PROTACs remain effective at lower doses, potentially reducing side effects [44, 61]. Second, unlike traditional drugs that rely on accessible binding pockets, PROTACs can target proteins previously considered undruggable and overcome resistance caused by mutations near active sites [15, 18]. However, the flexible ternary structure of PROTACs introduces a more complex structure-activity relationship, making modeling this process more challenging. The prediction of PROTAC-mediated degradation of a target protein \mathcal{P}^t by an E3 ligase can be formulated as:

$$f : \underbrace{(\text{Warhead, Linker, E3 ligand, E3 ligase, } \mathcal{P}^t)}_{\text{PROTAC}} \rightarrow \{0, 1\} \quad (2)$$

PROTACs Domain Models. Some initial efforts have been conducted to model the ternary complex formation induced by PROTAC molecules [8, 32]: DeepPROTACs employs GCNs to encode the ternary complex. ET-PROTAC considers the cross-talk between the PROTAC, target protein, and E3 ligase, which enables the modeling of the complex process in the targeted protein degradation.

Specialized Application 3: Protein-Ligand Interactions (PLI).

Application Description of PLI. As illustrated in Fig. 3, protein-ligand binding refers to the highly specific and affinity-driven interaction between a protein and a small molecule ligand, resulting in a stable complex that can block the binding of other molecules [42]. The binding affinity can be quantified by the Gibbs free energy change ΔG of the protein-ligand complex, where a more negative ΔG indicates stronger binding affinity. Accurate prediction of protein-ligand binding affinity enables efficient identification of promising drug candidates and accelerates the optimization of therapeutic molecules. For example, kinases play critical roles in regulating cell growth and survival pathways implicated in cancer. Thus, predicting kinase-ligand binding affinity facilitates the effective screening of kinase inhibitors, which can selectively block these pathways. The screened kinase inhibitors are promising candidates

for targeted cancer therapy. Predicting protein-ligand binding affinity can be formulated as a regression task: $f : (\mathcal{P}, \mathcal{M}) \rightarrow \mathbb{R}$, where \mathcal{P} denotes the protein and \mathcal{M} denotes the ligand molecule.

PLI Domain Models. Some domain-specific methods, such as MONN [34], do not rely on structural information. Instead, they predict atom-residue noncovalent interaction matrices as intermediate mechanistic signals to assist binding affinity prediction. To mitigate the false positive issue, KDBNet [37] applied an uncertainty recalibration technique to refine the uncertainty estimates.

General Application 4: Protein Function Annotation Prediction (PFA).

Application Description of PFA. To systematically represent protein functions, the Gene Ontology (GO) annotation framework was developed [3], providing structured annotations across Molecular Function (MF), Cellular Component (CC), and Biological Process (BP). E.g., in the Molecular Function (MF) aspect, a protein may be annotated with specific biochemical activities, such as immune response or signal transduction. Among the known protein sequences, fewer than 1% have experimentally validated functional annotations. Predicting the GO terms of proteins helps researchers better understand protein functions and potentially guide the discovery and design of proteins with desired functional properties.

PFA Domain Models. Protein function prediction is inherently a multi-label classification task. Early methods relied on sequence alignment or direct modeling of the sequence. More recent approaches have progressively integrated additional modalities. E.g., DeepFRI [20] combines protein structure and pre-trained sequence embeddings using a GCN, DPFunc [64] further incorporates domain-level information, and the PLM-based DeepGO-SE [29].

General Application 5: Mutation Effect Prediction for Protein Optimization (MTP).

Application Description of MTP. Protein mutations refer to the substitution, insertion, or deletion of amino acids within protein sequences. As illustrated in Fig. 3, mutations are frequently associated with changes in functional properties such as stability, binding affinity, and pathogenicity. Computational models can explore the protein fitness landscape to map sequences or structures to functional properties, which can enable protein optimization with mutations. For example, mutations in antibodies or protein complexes can be systematically explored to discover variants with enhanced binding affinity [7]. MTP can be formulated as estimating changes in target properties (e.g., stability changes measured by $\Delta\Delta G$) resulting from protein mutations. Due to limited experimental annotations, mutation effect prediction typically relies on a zero-shot learning setting.

MTP Domain Models. Recently, protein language models (PLMs) have shown promise in mutation effect prediction due to their ability to capture patterns learned from evolutionary data. PLMs tend to assign higher probabilities to mutations that are consistent with evolutionary patterns, and these mutations are more likely to yield beneficial functional effects. Details of the zero-shot mutation effective prediction with PLMs can be found in Appendix F.5.

Table 2: Comparisons across model architectures under different training strategies. The first line for each model (e.g., EGNN) denotes a randomly initialized protein encoder trained purely with downstream task supervision. The subsequent lines (e.g., w/MLM) represent pretrained encoders with frozen weights, where only the task-specific head is fine-tuned. Results of encoder finetuning are in Appendix D.3. Mutation effect prediction (MTP) is only applicable to masked language modeling.

Model	Specialized Tasks								General Tasks			
	PCS				PROTACs		PLI		PFA		MTP	
	C14.005		M10.003		ProtACDB Acc(%) \uparrow	AUC(%) \uparrow	Davis		MF		DMS	
	AUC(%) \uparrow	AUPR(%) \uparrow	AUC(%) \uparrow	AUPR(%) \uparrow			MSE \downarrow	Pear(%) \uparrow	Fmax(%) \uparrow	AUPR(%) \uparrow	Pear(%) \uparrow	AUC(%) \uparrow
EGNN	95.51 \pm 0.03	35.44 \pm 0.06	90.24 \pm 0.32	15.04 \pm 1.18	80.19 \pm 1.23	88.55 \pm 1.78	0.492 \pm 0.031	57.11 \pm 1.11	4.03 \pm 0.18	4.75 \pm 0.08	-	-
w/MLM	95.11 \pm 0.31	19.61 \pm 1.16	79.19 \pm 0.11	4.12 \pm 0.12	80.24 \pm 1.20	88.19 \pm 1.59	0.486 \pm 0.058	56.56 \pm 1.47	4.21 \pm 0.01	6.52 \pm 0.05	30.25	65.68
w/MVCL	94.80 \pm 0.00	19.61 \pm 1.16	82.84 \pm 0.68	3.23 \pm 0.13	78.78 \pm 2.57	86.02 \pm 1.00	0.510 \pm 0.035	52.68 \pm 5.15	4.13 \pm 0.01	5.78 \pm 0.00	-	-
w/PPF	95.09 \pm 0.41	27.95 \pm 0.99	82.45 \pm 0.73	5.43 \pm 0.87	79.72 \pm 1.44	87.64 \pm 1.01	0.483 \pm 0.013	55.74 \pm 1.92	9.06 \pm 0.18	8.23 \pm 0.09	-	-
SE(3) Trans	81.76 \pm 3.11	2.07 \pm 0.81	67.12 \pm 0.05	1.01 \pm 0.01	79.23 \pm 1.03	87.59 \pm 1.55	0.566 \pm 0.137	55.91 \pm 1.24	3.93 \pm 0.00	4.10 \pm 0.23	-	-
w/MLM	67.65 \pm 1.31	0.55 \pm 0.03	66.81 \pm 0.54	1.15 \pm 0.11	80.56 \pm 2.08	87.64 \pm 1.45	0.536 \pm 0.033	55.83 \pm 1.51	3.42 \pm 0.00	2.37 \pm 0.03	20.63	59.87
w/MVCL	44.01 \pm 0.72	0.20 \pm 0.00	52.16 \pm 2.50	0.53 \pm 0.07	68.11 \pm 5.57	77.84 \pm 2.23	0.819 \pm 0.164	48.42 \pm 2.86	3.39 \pm 0.00	2.38 \pm 0.01	-	-
w/PPF	69.27 \pm 2.53	0.81 \pm 0.17	66.24 \pm 3.13	1.20 \pm 0.16	79.24 \pm 1.16	87.53 \pm 1.07	0.539 \pm 0.038	52.06 \pm 2.30	3.55 \pm 0.06	2.58 \pm 0.10	-	-
GVP	95.55 \pm 0.46	17.99 \pm 5.02	86.05 \pm 1.68	5.40 \pm 0.52	70.67 \pm 1.42	77.58 \pm 1.12	0.516 \pm 0.007	49.52 \pm 2.59	5.41 \pm 0.11	2.15 \pm 0.03	-	-
w/MLM	93.23 \pm 0.34	8.31 \pm 0.87	80.94 \pm 0.45	4.03 \pm 0.11	70.03 \pm 2.16	77.51 \pm 1.07	0.524 \pm 0.007	48.52 \pm 2.62	9.21 \pm 0.26	4.05 \pm 0.12	20.78	60.65
w/MVCL	94.84 \pm 0.25	8.74 \pm 0.66	83.97 \pm 0.27	3.69 \pm 0.19	70.75 \pm 2.15	78.45 \pm 1.30	0.505 \pm 0.006	51.15 \pm 2.00	9.54 \pm 0.59	4.89 \pm 0.29	-	-
w/PPF	62.12 \pm 0.43	0.32 \pm 0.01	57.60 \pm 0.73	0.61 \pm 0.02	70.83 \pm 1.32	87.64 \pm 1.32	0.518 \pm 0.006	49.24 \pm 1.15	10.12 \pm 0.07	5.30 \pm 0.02	-	-
ProtBERT	95.49 \pm 0.09	40.49 \pm 0.25	89.83 \pm 0.05	10.74 \pm 0.12	75.38 \pm 1.51	84.13 \pm 1.89	0.521 \pm 0.020	50.23 \pm 1.24	3.39 \pm 0.00	2.93 \pm 0.01	-	-
w/MLM	95.45 \pm 0.10	9.37 \pm 0.62	85.56 \pm 0.76	7.12 \pm 0.06	78.20 \pm 1.14	86.75 \pm 1.78	0.519 \pm 0.033	52.67 \pm 1.13	4.15 \pm 0.01	4.27 \pm 0.01	14.20	60.92
w/MVCL	95.78 \pm 0.21	28.51 \pm 0.06	86.13 \pm 0.19	7.16 \pm 0.39	79.06 \pm 2.71	86.45 \pm 1.08	0.553 \pm 0.049	55.82 \pm 1.67	3.51 \pm 0.00	4.66 \pm 0.03	-	-
w/PPF	64.25 \pm 0.35	0.36 \pm 0.00	57.29 \pm 0.10	0.67 \pm 0.01	80.51 \pm 1.03	87.46 \pm 1.71	0.533 \pm 0.048	54.81 \pm 2.08	6.05 \pm 0.05	5.64 \pm 0.01	-	-
D-Trans	97.60 \pm 0.08	61.42 \pm 1.30	88.28 \pm 0.79	22.82 \pm 2.95	80.08 \pm 1.08	86.58 \pm 0.28	0.416 \pm 1.028	60.92 \pm 0.22	19.57 \pm 0.80	11.16 \pm 0.67	-	-
w/MLM	96.53 \pm 0.52	20.12 \pm 2.86	84.10 \pm 0.66	11.73 \pm 1.41	77.78 \pm 1.93	85.16 \pm 0.89	0.494 \pm 1.116	55.79 \pm 0.50	17.92 \pm 0.14	9.85 \pm 0.09	-0.09	56.84
w/MVCL	95.23 \pm 0.46	41.26 \pm 10.3	83.50 \pm 0.79	15.85 \pm 1.30	74.16 \pm 1.44	82.32 \pm 0.81	0.550 \pm 2.620	54.21 \pm 0.08	15.87 \pm 0.26	8.00 \pm 0.20	-	-
w/PPF	96.40 \pm 0.59	39.56 \pm 5.55	85.51 \pm 0.42	12.29 \pm 1.26	74.76 \pm 1.08	82.34 \pm 0.09	0.445 \pm 1.064	56.46 \pm 0.01	17.46 \pm 0.18	9.46 \pm 0.12	-	-
ESM-2	97.23 \pm 0.06	41.22 \pm 0.25	86.34 \pm 0.12	6.16 \pm 0.07	78.46 \pm 3.03	85.74 \pm 3.47	0.491 \pm 4.823	53.25 \pm 1.26	49.79 \pm 0.03	43.44 \pm 0.17	43.05	73.48
ESM-C	95.76 \pm 0.01	38.28 \pm 0.08	88.08 \pm 0.00	8.06 \pm 0.08	80.47 \pm 0.90	86.74 \pm 0.37	0.461 \pm 0.037	53.41 \pm 0.87	38.27 \pm 0.16	30.31 \pm 0.12	42.51	73.24
SaProt	96.16 \pm 0.16	42.91 \pm 0.27	89.18 \pm 0.06	13.48 \pm 0.03	73.44 \pm 1.32	80.29 \pm 0.70	0.473 \pm 0.004	51.66 \pm 0.67	33.06 \pm 0.09	25.21 \pm 0.11	49.22	76.89

5 Experiments

In this section, we conduct empirical studies to compare domain models and various pretraining frameworks and strategies on the downstream applications described in Sec. 4.

5.1 Experimental Setup

5.1.1 Pretraining Setup. We describe the pretraining setting here. **Pretraining Dataset.** For pre-training, we collect 542,378 protein structures from AlphaFold Protein Structure Database (AFDB) and obtain the corresponding amino acid sequences and protein family labels from UniProt [10, 62]. This curated dataset spans diverse and non-redundant protein structures, enabling a comprehensive evaluation of different training strategies. ESM-2 and SaProt are trained on protein sequences from UniRef [10], while ESM-C further incorporates sequences from MGnify [52] and the JGI [45]. Additional dataset details are provided in Appendix G.2.

Model Setups. We use fixed random seeds 42, 128, 256, 512, 1024 for reproducibility, and report mean \pm standard deviation over five runs. All models are trained with the Adam optimizer. The learning rate follows a linear warm-up over 10% of training steps, then cosine annealing to $1e-6$, with a peak of $1e-4$. More training details are provided in Appendix F.

5.1.2 Downstream Task Training Setup. In this subsection, we introduce the setup of training pretrained models and domain models for downstream application tasks.

Downstream Application Dataset. Each downstream task uses the same dataset for both training-from-scratch and fine-tuning

to ensure fair comparison. All datasets are collected from peer-reviewed sources and standardized through quality control and formatting, as detailed in Appendix F. Specifically, PROTACs data are from PROTAC-DB [19], cleavage data from MEROPS [51], protein-ligand interactions from KDBNet, function prediction from DeepFRI [20] (with structural data from ProteinWorkshop [26]), and mutation prediction from ProteinGym [47].

Molecular Encoders in Downstream Applications. The applications of PLI and PROTACs involve various chemical molecules in the interactions with proteins, requiring a molecular encoder. To maintain consistency and comparability across interaction tasks, molecular components, drugs in PLI, warheads, linkers, and E3-ligands in PROTACs are encoded using randomly initialized GVP encoders and updated under all training settings. For domain-specific models, molecular encoders follow their original implementations. **Downstream Task Training Strategies.** All domain-specific models are trained from scratch. Pretrained models serve as protein encoders under the following training settings:

- **Training from scratch:** All parameters are randomly initialized and trained end-to-end.
- **Freeze-encoder training:** Encoders are initialized with pretrained weights and kept frozen, while only task-specific heads and molecular encoders are updated.
- **Multi-stage fine-tuning:** The protein encoder initialized with pretrained weights is first frozen to train the task-specific heads and molecular encoders, followed by fine-tuning the entire model using a smaller learning rate.

Evaluation. We evaluate all methods on the five downstream applications in Protap using task-standard metrics which are shown in Table. 1a. Detailed criteria for selecting these metrics are provided in Appendix F.

Table 3: Summary of best results in different pretrain objectives under each fine-tuning strategy.

Model	Fine-tuning strategy	PCS	PROTACs	PLI
		C14.005 AUC(%) \uparrow	PROTACDB AUC(%) \uparrow	Davis MSE \downarrow
EGNN	From scratch	95.51 \pm 0.03	88.55 \pm 1.78	0.492 \pm 0.031
	Frozen encoder	95.11 \pm 0.31	88.19 \pm 1.59	0.482 \pm 0.022
	Multi-stage	95.72 \pm 0.14	88.96 \pm 1.42	0.501 \pm 0.025
D-Trans	From scratch	97.60 \pm 0.08	86.58 \pm 0.28	0.416 \pm 1.028
	Frozen encoder	96.53 \pm 0.52	85.16 \pm 0.89	0.445 \pm 1.064
	Multi-stage	98.11 \pm 0.00	85.53 \pm 0.61	0.425 \pm 0.029
ProtBERT	From scratch	95.49 \pm 0.09	84.13 \pm 1.89	0.521 \pm 0.020
	Frozen encoder	95.78 \pm 0.21	87.46 \pm 1.71	0.519 \pm 0.033
	Multi-stage	95.80 \pm 0.02	88.00 \pm 0.97	0.519 \pm 0.017
ESM-2	Frozen encoder	97.23 \pm 0.06	85.74 \pm 3.47	0.491 \pm 4.823
	Multi-stage	98.16 \pm 0.03	89.96 \pm 1.49	0.404 \pm 0.010

5.2 Analysis on Protein Model Pretraining

In this section, we examine three pretraining tasks employed in Protap as described in Sec. 3.2, which are MLM, MVCL, and PFP. We pre-train EGNN, SE(3) Transformer (SE(3) Trans), GVP, ProteiBERT (ProtBERT), and D-Transformer (D-Trans) with all three tasks with 542k proteins to obtain pretraining encoders, which are listed in Tab. 1 and are detailed in Appendix G. For ESM-2 and ESM-C, we testify to the publicly released pretrained weights that are learned via MLM training on 70M proteins. In particular, we aim to make comparisons across the following aspects:

RQ1 Scaling Law on Protein Modeling: *Can large-scale pre-training encoders outperform a supervised encoder that trained on the small downstream training set from scratch?*

Compared with Frozen Pretraining Encoders. The results of frozen pretraining encoders and supervised encoders are given in Table. 2, we observe that: (i) the unsupervised pretraining encoders can achieve competitive performance on various downstream tasks. For example, using frozen pretraining encoders of ESM-2 and SaProt often outperform supervised encoders (e.g., EGNN, SE(3) Trans, and ProtBert) on downstream tasks. (ii) However, current supervised encoders trained from scratch tend to outperform the unsupervised pretraining encoders even when they are trained with large-scale datasets. For example, the supervised encoder of D-Trans generally outperforms all other unsupervised encoders. This implies a degree of mismatch between the pretraining objectives and the downstream tasks, indicating that training from scratch enables the model to learn task-specific representations that are more aligned with the requirements of the downstream task.

Compared with Finetuned Pretraining Encoders. As shown in Tab. 3, by including the results of multi-stage fine-tuning in comparison, we find that multi-stage fine-tuning almost consistently outperforms the from-scratch and frozen-encoder setting, and the benefit becomes more pronounced as interaction complexity increases, particularly in PCS and PROTACs, where enzyme-substrate

contact and ternary alignment require coordinating multiple interacting entities. These results indicate that for protein modeling tasks involving cross-modal alignment, effective use of pretrained models requires not only preserving pretrained knowledge but also providing the necessary representation adaptation capacity.

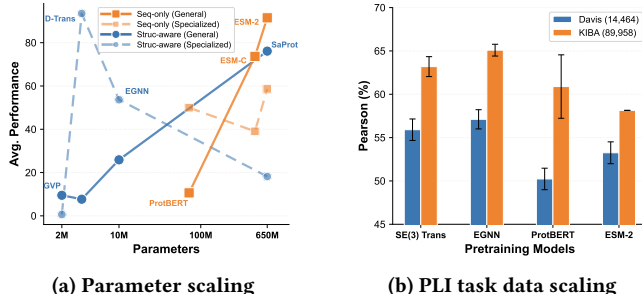


Figure 5: Scaling behavior in parameters and training data

Analysis of Scaling Law on Proteins. We analyze protein scaling laws from three perspectives. (i) Pre-train data scaling. As shown in Fig. 5(a), increasing the scale of pre-training data provides limited gains for specialized tasks. Models pre-trained on billions of sequences, such as the ESM family, do not consistently outperform those trained on much smaller corpora, and may even exhibit degraded performance. In contrast, large-scale pre-training yields clear improvements on general tasks, likely reflecting enhanced capture of protein evolutionary signals. (ii) Model parameter scaling. Fig. 5(a) reveals a pronounced model-size scaling law for general tasks, with performance steadily improving as model size increases from 2M to 650M parameters (e.g., ESM2 vs. ProteinBERT). However, this trend largely vanishes on specialized tasks such as PROTACs. (iii) Domain data scaling. Fig. 5(b) shows that downstream data scale also exhibits a power-law behavior: expanding the PLI dataset from approximately 14k to nearly 100k samples leads to substantial performance gains, which highlights that task-specific data plays a vital role in realizing scaling benefits.

RQ2 Sequential or Structural Models: *Are models incorporating structures better than those purely using protein sequences?*

As shown in Fig. 6, we observe that on specialized applications, the models with lower average ranks are all structure-aware models. For general tasks such as PFA and MTP that rely more on evolutionary and semantic statistical regularities, large-scale PLMs trained on much larger corpora show clear advantages. However, when controlling for training data scale and model capacity (E.g., ProtBERT vs. others), most structure-aware models still outperform the sequence-only model. These observations highlight two key insights: (i) incorporating three-dimensional structural information introduces essential inductive biases that are missing in sequence-only architectures. (ii) For tasks where performance depends strongly on geometric constraints, binding interfaces and pockets, and complex interactions, structural information can be more important than parameter scale to some extent.

RQ3 Pretraining Tasks: *Is there any pretraining task that consistently outperforms others on downstream tasks?*

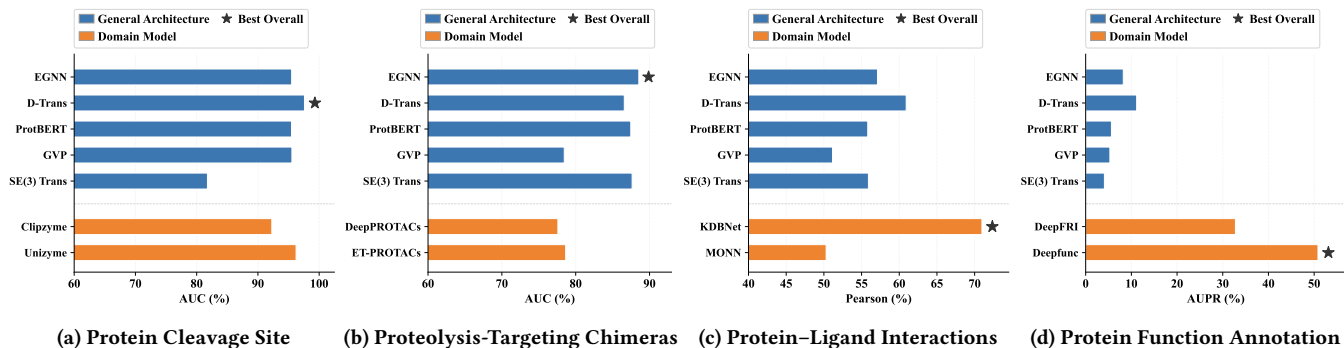


Figure 4: Performance comparison between general architecture and domain-specific models across downstream applications.

To quantitatively assess whether any pretraining objective consistently outperforms others, we conduct rank-based Friedman tests with Nemenyi post-hoc analyses across all five model architectures, comparing three pretraining strategies. The results show that although the overall Friedman test reaches significance ($\chi^2=6.10$, $p=0.047$), the concordance is low ($W=0.153$), indicating limited agreement across model-task blocks; accordingly, no pairwise difference is significant under Nemenyi ($CD=0.741$, $\alpha=0.05$). Per-task Friedman tests show no significant differences on PCS, PROTACs, or PLI. The sole exception is PFA, where PFP achieves the best average rank (Friedman $\chi^2=6.40$, $p=0.041$) and significantly outperforms MVCL in the Nemenyi test ($|\Delta R|=1.60 > CD=1.48$). Detailed results are presented in Tab. 9. Overall, these results suggest no universal advantage of a single pretraining objective, while PFP specifically benefits functional annotation.

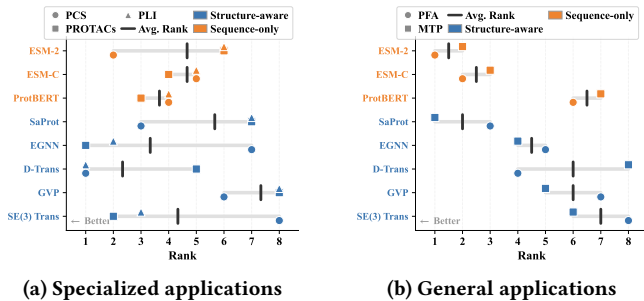


Figure 6: Performance ranking of structure-aware and sequence-only models on downstream applications.

5.3 Analysis on Domain Models

We compare the pretraining model architectures with eight domain-specific models, which are listed in Tab. 1. Since the representative solution of mutation effect prediction is protein language models, we omit the comparison on mutation effect prediction. For the pretraining model architectures, we report the best-performing training strategies according to Tab. 2. The comparison between pretrained model architectures and domain-specific architectures is presented in Fig. 4 (a)–(d). In particular, we aim to answer the following research questions.

RQ4: Domain Model or General Encoder: *How do the domain-specific models perform compared with general ones?*

The performance of domain-specific models and pretrained models varies across different tasks. We observe that on the protein-ligand interaction and protein function annotation prediction task, the domain-specific models could outperform the general model architectures by a large margin. However, for the applications of PROTACs that exhibit complex interaction processes, the general framework EGNN exhibits great results. SaProt greatly outperforms other models in mutation effects prediction, including ESM-2. This is likely attributable to the Structure-Vocabulary, which reduces local sequence ambiguity and mitigates semantic confusion.

RQ5: Effect of Biochemical and Structural Priors: *To what extent does incorporating biochemical or structural inductive biases improve generalization across downstream applications?*

We observe that several domain-specific models outperform, or are comparable to, general-purpose models, including UniZyme, DeepFunc, DeepFRI, and KDBNet. In contrast, models relying only on 2D cues or sequence features, such as MONN, DeepPROTACs, and ET-PROTACs, consistently perform the worst. Notably, the strong domain models share two common traits: they leverage pretrained representations for initialization or feature enhancement, and they incorporate task-aligned priors, such as family information for PFA and energy-frustration signals for PCS. These findings suggest that pretrained representations can effectively strengthen domain models, while prior knowledge should be carefully chosen to match the data and task.

6 Conclusion and Future Works

We introduce Protap, a unified benchmark that brings together general-purpose pretraining architectures and domain-specific models to evaluate five key protein modeling applications under a standard, reproducible framework. Our extensive experiments indicate that no single model or pretraining objective can outperform all others across applications. There are two directions that need further investigation: (i) We will further explore the scaling laws that govern how model capacity and pretraining data volume translate into downstream gains. (ii) We will extend Protap to holistically cover protein design tasks, e.g., peptide design, enzyme design.

References

- [1] Josh Achiam, Steven Adler, Sandhini Agarwal, Lama Ahmad, Ilge Akkaya, Florencia Leoni Aleman, Diogo Almeida, Janko Altmenschmidt, Sam Altman, Shyamal Anadkat, et al. 2023. Gpt-4 technical report.
- [2] Christian B Anfinsen. 1973. Principles that govern the folding of protein chains. *Science* 181, 4096 (1973), 223–230.
- [3] Michael Ashburner, Catherine A Ball, Judith A Blake, David Botstein, Heather Butler, J Michael Cherry, Allan P Davis, Kara Dolinski, Selina S Dwight, Janan T Eppig, et al. 2000. Gene ontology: tool for the unification of biology. *Nature genetics* 25, 1 (2000), 25–29.
- [4] Harry P Austin, Mark D Allen, Bryon S Donohoe, Nicholas A Rorrer, Fiona L Kearns, Rodrigo L Silveira, Benjamin C Pollard, Graham Dominick, Ramona Duman, Kamel El Omari, et al. 2018. Characterization and engineering of a plastic-degrading aromatic polyesterase. *Proceedings of the National Academy of Sciences (PNAS)* 115, 19 (2018), E4350–E4357.
- [5] Alex Bateman, Lachlan Coin, Richard Durbin, Robert D Finn, Volker Hollich, Sam Griffiths-Jones, Ajay Khanna, Mhairi Marshall, Simon Moxon, Erik LL Sonnhammer, et al. 2004. The Pfam protein families database. *Nucleic acids research* 32, suppl_1 (2004), D138–D141.
- [6] Nadav Brandes, Dan Ofer, Yam Peleg, Nadav Rappoport, and Michal Linial. 2022. ProteinBERT: a universal deep-learning model of protein sequence and function. *Bioinformatics* 38, 8 (2022), 2102–2110.
- [7] Huiyu Cai, Zuobai Zhang, Mingkai Wang, Bozitao Zhong, Quanxiao Li, Yuxuan Zhong, Yanling Wu, Tianlei Ying, and Jian Tang. 2024. Pretrainable geometric graph neural network for antibody affinity maturation. *Nature communications* (2024).
- [8] Lijun Cai, Guanyu Yue, Yifan Chen, Li Wang, Xiaojun Yao, Quan Zou, Xiangzheng Fu, and Dongsheng Cao. 2025. ET-PROTACs: modeling ternary complex interactions using cross-modal learning and ternary attention for accurate PROTAC-induced degradation prediction. *Briefings in Bioinformatics* 26, 1 (2025), bbae654.
- [9] Henriette Capel, Robin Weiler, Maurits Dijkstra, Reinier Vlegels, Peter Bloem, and K Anton Feenstra. 2022. ProteinGLUE multi-task benchmark suite for self-supervised protein modeling. *Scientific Reports* (2022).
- [10] UniProt Consortium. 2019. UniProt: a worldwide hub of protein knowledge. *Nucleic acids research* (2019).
- [11] J. Dauparas, I. Anishchenko, N. Bennett, H. Bai, R. J. Ragotte, L. F. Milles, B. I. M. Wicky, A. Courbet, R. J. de Haas, N. Bethel, P. J. Y. Leung, T. F. Huddy, S. Pellock, D. Tischer, F. Chan, B. Koepnick, H. Nguyen, A. Kang, B. Sankaran, A. K. Bera, N. P. King, and D. Baker. 2022. Robust deep learning-based protein sequence design using ProteinMPNN. *Science* (2022).
- [12] Mindy I Davis, Jeremy P Hunt, Sanna Herrgard, Pietro Ciceri, Lisa M Wodicka, Gabriel Pallares, Michael Hocker, Daniel K Treiber, and Patrick P Zarrinkar. 2011. Comprehensive analysis of kinase inhibitor selectivity. *Nature biotechnology* (2011).
- [13] Jacob Devlin, Ming-Wei Chang, Kenton Lee, and Kristina Toutanova. 2019. Bert: Pre-training of deep bidirectional transformers for language understanding. In *Proceedings of the Conference of the North American Chapter of the Association for Computational Linguistics (NAACL)*.
- [14] Sean R Eddy. 2004. Where did the BLOSUM62 alignment score matrix come from? *Nature biotechnology* (2004).
- [15] Scott D Edmondson, Bin Yang, and Charlene Fallan. 2019. Proteolysis targeting chimeras (PROTACs) in 'beyond rule-of-five' chemical space: Recent progress and future challenges. *Bioorganic & Medicinal Chemistry Letters* (2019).
- [16] Ahmed Elnaggar, Michael Heinzinger, Christian Dallago, Ghalia Rehawi, Yu Wang, Llion Jones, Tom Gibbs, Tamas Feher, Christoph Angerer, Martin Steinegger, et al. 2021. ProtTrans: Toward understanding the language of life through self-supervised learning. *IEEE transactions on pattern analysis and machine intelligence (TPAMI)* (2021).
- [17] Fabian Fuchs, Daniel Worrall, Volker Fischer, and Max Welling. 2020. Se (3)-transformers: 3d roto-translation equivariant attention networks. *Advances in Neural Information Processing Systems (NeurIPS)* (2020).
- [18] K Garber. 2022. The PROTAC gold rush. *Nature biotechnology* (2022).
- [19] Jingxuan Ge, Shimeng Li, Gaoqi Weng, Huating Wang, Meijing Fang, Huiyong Sun, Yafeng Deng, Chang-Yu Hsieh, Dan Li, and Tingjun Hou. 2025. PROTAC-DB 3.0: an updated database of PROTACs with extended pharmacokinetic parameters. *Nucleic acids research* (2025).
- [20] Vladimir Gligorijević, P Douglas Renfrew, Tomasz Kosciolk, Julia Koehler Leman, Daniel Berenberg, Tommi Vatanen, Chris Chandler, Bryn C Taylor, Ian M Fisk, Hera Vlamakis, et al. 2021. Structure-based protein function prediction using graph convolutional networks. *Nature communications* (2021).
- [21] Thomas Hayes, Roshan Rao, Halil Akin, Nicholas J Sofroniew, Deniz Oktay, Zeming Lin, Robert Verkuil, Vincent Q Tran, Jonathan Deaton, Marius Wiggert, et al. 2025. Simulating 500 million years of evolution with a language model. *Science* (2025).
- [22] Dan Hendrycks and Kevin Gimpel. 2016. Gaussian error linear units (gelus). *arXiv Preprint* (2016).
- [23] Sepp Hochreiter and Jürgen Schmidhuber. 1997. Long short-term memory. *Neural computation* (1997).
- [24] Weihua Hu, Bowen Liu, Joseph Gomes, Marinka Zitnik, Percy Liang, Vijay Pande, and Jure Leskovec. 2020. Strategies for Pre-training Graph Neural Networks. In *International Conference on Learning Representations (ICLR)*.
- [25] John Ingraham, Vikas Garg, Regina Barzilay, and Tommi Jaakkola. 2019. Generative models for graph-based protein design. In *Advances in Neural Information Processing Systems (NeurIPS)*.
- [26] Arian Rokkum Jamasb, Alex Morehead, Chaitanya K. Joshi, Zuobai Zhang, Kieran Didi, Simon V Mathis, Charles Harris, Jian Tang, Jianlin Cheng, Pietro Lio, and Tom Leon Blundell. 2024. Evaluating Representation Learning on the Protein Structure Universe. In *International Conference on Learning Representations (ICLR)*.
- [27] Bowen Jing, Stephan Eismann, Patricia Suriana, Raphael John Lamarre Townsend, and Ron Dror. 2021. Learning from Protein Structure with Geometric Vector Perceptrons. In *International Conference on Learning Representations (ICLR)*.
- [28] Thomas N Kipf and Max Welling. 2017. Semi-Supervised Classification with Graph Convolutional Networks. In *International Conference on Learning Representations (ICLR)*.
- [29] Maxat Kulmanov, Francisco J Guzmán-Vega, Paula Duek Roggli, Lydie Lane, Stefan T Arold, and Robert Hoehndorf. 2024. Protein function prediction as approximate semantic entailment. *Nature machine intelligence* (2024).
- [30] Youhan Lee, Hasun Yu, Jaemyung Lee, and Jaehoon Kim. 2024. Pre-training Sequence, Structure, and Surface Features for Comprehensive Protein Representation Learning. In *International Conference on Learning Representations (ICLR)*.
- [31] Chenao Li, Shuo Yan, and Enyan Dai. 2025. UniZyme: A Unified Protein Cleavage Site Predictor Enhanced with Enzyme Active-Site Knowledge. In *Advances in Neural Information Processing Systems (NeurIPS)*.
- [32] Fenglei Li, Qiaoyu Hu, Xianglei Zhang, Renhong Sun, Zhuanghua Liu, Sanan Wu, Siyuan Tian, Xinyue Ma, Zhizhuo Dai, Xiaobao Yang, et al. 2022. DeepPROTACs is a deep learning-based targeted degradation predictor for PROTACs. *Nature communications* (2022).
- [33] Fuyi Li, Andre Leier, Quanzhong Liu, Yanan Wang, Dongxu Xiang, Tatsuya Akutsu, Geoffrey I Webb, A Ian Smith, Tatiana Marquez-Lago, Jian Li, et al. 2020. Procleave: predicting protease-specific substrate cleavage sites by combining sequence and structural information. *Genomics, proteomics & bioinformatics* (2020).
- [34] Shuya Li, Fangping Wan, Hantao Shu, Tao Jiang, Dan Zhao, and Jianyang Zeng. 2020. MONN: A Multi-objective Neural Network for Predicting Compound-Protein Interactions and Affinities. *Cell systems* (2020).
- [35] Zeming Lin, Halil Akin, Roshan Rao, Brian Hie, Zhongkai Zhu, Wenting Liu, Nikita Smetanin, Robert Verkuil, Ori Kabeli, Yaniv Shmueli, et al. 2023. Evolutionary-scale prediction of atomic-level protein structure with a language model. *Science* (2023).
- [36] Shengjie Luo, Tianlang Chen, Yixian Xu, Shuxin Zheng, Tie-Yan Liu, Liwei Wang, and Di He. 2023. One Transformer Can Understand Both 2D & 3D Molecular Data. In *International Conference on Learning Representations (ICLR)*.
- [37] Yunan Luo, Yang Liu, and Jian Peng. 2023. Calibrated geometric deep learning improves kinase-drug binding predictions. *Nature machine intelligence* (2023).
- [38] Zhengtong Lv, Yuan Chu, and Yong Wang. 2015. HIV protease inhibitors: a review of molecular selectivity and toxicity. *HIV/AIDS-Research and palliative care* (2015).
- [39] Craig O Mackenzie and Gevorg Grigoryan. 2017. Protein structural motifs in prediction and design. *Current opinion in structural biology* (2017).
- [40] Hadir Marei, Wen-Ting K Tsai, Yee-Seir Kee, Karen Ruiz, Jieyan He, Chris Cox, Tao Sun, Sai Penikalapati, Pankaj Dwivedi, Meena Choi, et al. 2022. Antibody targeting of E3 ubiquitin ligases for receptor degradation. *Nature* (2022).
- [41] Peter Mikhael, Itamar Chinn, and Regina Barzilay. 2024. CLIPZyme: Reaction-Conditioned Virtual Screening of Enzymes. In *International Conference on Machine Learning (ICML)*.
- [42] David W Miller and Ken A Dill. 1997. Ligand binding to proteins: the binding landscape model. *Protein science* (1997).
- [43] Seonwoo Min, Seunghyun Park, Siwon Kim, Hyun-Soo Choi, Byunghan Lee, and Sungroh Yoon. 2021. Pre-training of deep bidirectional protein sequence representations with structural information. *IEEE Access* (2021).
- [44] Taavi K Neklesa, James D Winkler, and Craig M Crews. 2017. Targeted protein degradation by PROTACs. *Pharmacology & therapeutics* (2017).
- [45] Henrik Nordberg, Michael Cantor, Serge Dusheyko, Susan Hua, Alexander Poliakov, Igor Shabalov, Tatyana Smirnova, Igor V Grigoriev, and Inna Dubchak. 2014. The genome portal of the Department of Energy Joint Genome Institute: 2014 updates. *Nucleic acids research* (2014).
- [46] Pascal Notin, Mafalda Dias, Jonathan Frazer, Javier Marchena-Hurtado, Aidan N Gomez, Debora Marks, and Yarin Gal. 2022. Tranception: protein fitness prediction with autoregressive transformers and inference-time retrieval. In *International Conference on Machine Learning (ICML)*.
- [47] Pascal Notin, Aaron Kollasch, Daniel Ritter, Lood Van Niekerk, Steffanie Paul, Han Spinner, Nathan Rollins, Ada Shaw, Rose Orenbuch, Ruben Weitzman, et al. 2023. Proteingym: Large-scale benchmarks for protein fitness prediction and

- design. *Advances in Neural Information Processing Systems (NeurIPS)* (2023).
- [48] Chris P Ponting and Robert R Russell. 2002. The natural history of protein domains. *Annual review of biophysics and biomolecular structure* (2002).
- [49] Alec Radford, Jong Wook Kim, Chris Hallacy, Aditya Ramesh, Gabriel Goh, Sandhini Agarwal, Girish Sastry, Amanda Askell, Pamela Mishkin, Jack Clark, et al. 2021. Learning transferable visual models from natural language supervision. In *International Conference on Machine Learning (ICML)*.
- [50] Roshan Rao, Nicholas Bhattacharya, Neil Thomas, Yan Duan, Peter Chen, John Canny, Pieter Abbeel, and Yun Song. 2019. Evaluating protein transfer learning with TAPE. *Advances in Neural Information Processing Systems (NeurIPS)* (2019).
- [51] Neil D Rawlings, Matthew Waller, Alan J Barrett, and Alex Bateman. 2014. MEROPS: the database of proteolytic enzymes, their substrates and inhibitors. *Nucleic acids research* (2014).
- [52] Lorna Richardson, Ben Allen, Germana Baldi, Martin Beracochea, Maxwell L Bileschi, Tony Burdett, Josephine Burgin, Juan Caballero-Pérez, Guy Cochrane, Lucy J Colwell, et al. 2023. MGnify: the microbiome sequence data analysis resource in 2023. *Nucleic acids research* (2023).
- [53] Adam J Riesselman, John B Ingraham, and Debora S Marks. 2018. Deep generative models of genetic variation capture the effects of mutations. *Nature methods* (2018).
- [54] Alexander Rives, Joshua Meier, Tom Sercu, Siddharth Goyal, Zeming Lin, Jason Liu, Demi Guo, Myle Ott, C Lawrence Zitnick, Jerry Ma, et al. 2021. Biological structure and function emerge from scaling unsupervised learning to 250 million protein sequences. *Proceedings of the National Academy of Sciences (PNAS)* (2021).
- [55] Arman A Sadybekov, Anastasiia V Sadybekov, Yongfeng Liu, Christos Iliopoulos-Tsoutsouvas, Xi-Ping Huang, Julie Pickett, Blake Houser, Nilkanth Patel, Ngan K Tran, Fei Tong, et al. 2022. Synthon-based ligand discovery in virtual libraries of over 11 billion compounds. *Nature* (2022).
- [56] Victor Garcia Satorras, Emiel Hoogeboom, and Max Welling. 2021. E (n) equivariant graph neural networks. In *International Conference on Machine Learning (ICML)*.
- [57] Ian Sillitoe, Nicola Bordin, Natalie Dawson, Vaishali P Waman, Paul Ashford, Harry M Scholes, Camilla SM Pang, Laurel Woodriddle, Clemens Rauer, Neeladri Sen, et al. 2021. CATH: increased structural coverage of functional space. *Nucleic acids research* (2021).
- [58] Jin Su, Chenchen Han, Yuyang Zhou, Junjie Shan, Xibin Zhou, and Fajie Yuan. 2024. SaProt: Protein Language Modeling with Structure-aware Vocabulary. In *International Conference on Learning Representations (ICLR)*.
- [59] Jing Tang, Agnieszka Szwajda, Sushil Shakyawar, Tao Xu, Petteri Hintsanen, Krister Wennerberg, and Tero Aittokallio. 2014. Making sense of large-scale kinase inhibitor bioactivity data sets: a comparative and integrative analysis. *Journal of chemical information and modeling* (2014).
- [60] Nathaniel Thomas, Tess Smidt, Steven Kearnes, Lusann Yang, Li Li, Kai Kohlhoff, and Patrick Riley. 2018. Tensor field networks: Rotation-and translation-equivariant neural networks for 3d point clouds. *arXiv Preprint* (2018).
- [61] Momar Toure and Craig M Crews. 2016. Small-molecule PROTACS: new approaches to protein degradation. *Angewandte Chemie International Edition* (2016).
- [62] Mihaly Varadi, Stephen Anyango, Mandar Deshpande, Sreenath Nair, Cindy Natassia, Galabina Yordanova, David Yuan, Oana Stroe, Gemma Wood, Agata Laydon, et al. 2022. AlphaFold Protein Structure Database: massively expanding the structural coverage of protein-sequence space with high-accuracy models. *Nucleic acids research* (2022).
- [63] Ashish Vaswani, Noam Shazeer, Niki Parmar, Jakob Uszkoreit, Llion Jones, Aidan N Gomez, Łukasz Kaiser, and Illia Polosukhin. 2017. Attention is all you need. *Advances in Neural Information Processing Systems (NeurIPS)* (2017).
- [64] Wenkang Wang, Yunyan Shuai, Min Zeng, Wei Fan, and Min Li. 2025. DPFunc: accurately predicting protein function via deep learning with domain-guided structure information. *Nature communications* (2025).
- [65] Felix Wong, Erica J Zheng, Jacqueline A Valeri, Nina M Donghia, Melis N Anahar, Satotaka Omori, Alicia Li, Andres Cubillos-Ruiz, Aarti Krishnan, Wengong Jin, et al. 2024. Discovery of a structural class of antibiotics with explainable deep learning. *Nature* (2024).
- [66] Jiangxia Wu, Yihao Chen, Jingxing Wu, Duancheng Zhao, Jindi Huang, Mujie Lin, and Ling Wang. 2024. Large-scale comparison of machine learning methods for profiling prediction of kinase inhibitors. *Journal of Cheminformatics* (2024).
- [67] Ruidong Wu, Fan Ding, Rui Wang, Rui Shen, Xiwen Zhang, Shitong Luo, Chenpeng Su, Zuofan Wu, Qi Xie, Bonnie Berger, et al. 2022. High-resolution de novo structure prediction from primary sequence. *BioRxiv* (2022).
- [68] Minghao Xu, Zuobai Zhang, Jiarui Lu, Zhaocheng Zhu, Yangtian Zhang, Ma Chang, Runcheng Liu, and Jian Tang. 2022. Peer: a comprehensive and multi-task benchmark for protein sequence understanding. *Advances in Neural Information Processing Systems (NeurIPS)* (2022).
- [69] Kevin Yang, Kyle Swanson, Wengong Jin, Connor Coley, Philipp Eiden, Hua Gao, Angel Guzman-Perez, Timothy Hopper, Brian Kelley, Miriam Mathea, et al. 2019. Analyzing learned molecular representations for property prediction. *Journal of chemical information and modeling* (2019).
- [70] Fei YE, Zaixiang Zheng, Dongyu Xue, Yuning Shen, Lihao Wang, Yiming Ma, Yan Wang, Xinyou Wang, Xiangxin Zhou, and Quanquan Gu. 2025. ProteinBench: A Holistic Evaluation of Protein Foundation Models. In *International Conference on Learning Representations (ICLR)*.
- [71] Chengxuan Ying, Tianle Cai, Shengjie Luo, Shuxin Zheng, Guolin Ke, Di He, Yanming Shen, and Tie-Yan Liu. 2021. Do transformers really perform badly for graph representation? *Advances in Neural Information Processing Systems (NeurIPS)* (2021).
- [72] Kang Zhang, Xin Yang, Yifei Wang, Yunfang Yu, Niu Huang, Gen Li, Xiaokun Li, Joseph C Wu, and Shengyong Yang. 2025. Artificial intelligence in drug development. *Nature Medicine* (2025).
- [73] Ningyu Zhang, Zhen Bi, Xiaozhuan Liang, Siyuan Cheng, Haosen Hong, Shumin Deng, Qiang Zhang, Jiazhang Lian, and Huajun Chen. 2022. OntoProtein: Protein Pretraining With Gene Ontology Embedding. In *International Conference on Learning Representations (ICLR)*.
- [74] Zuobai Zhang, Minghao Xu, Arian Rokkum Jamsab, Vijil Chenthamarakshan, Aurelie Lozano, Payel Das, and Jian Tang. 2023. Protein Representation Learning by Geometric Structure Pretraining. In *International Conference on Learning Representations (ICLR)*.

A Abbreviation Statement

The Tab.4 lists the abbreviations used throughout the paper, covering downstream applications, pretraining objectives, model architectures, datasets, and biological terminology.

Table 4: List of abbreviations used in this paper.

Abbreviation	Description
<i>Downstream Applications</i>	
PCS	Protein Cleavage Site prediction
PROTACs	Proteolysis-Targeting Chimeras
PLI	Protein-Ligand Interaction
PFA	Protein Function Annotation
MTP	Mutation Effect Prediction
<i>Pretraining Objectives</i>	
MLM	Masked Language Modeling
MVCL	Multi-View Contrastive Learning
PPF	Protein Family Prediction
<i>Models & Architectures</i>	
EGNN	Equivariant Graph Neural Network
SE(3) Trans	SE(3)-Equivariant Transformer
GVP	Geometric Vector Perceptron
D-Trans	Distance-aware Transformer
ProtBERT	ProteinBERT
ESM-C	ESM Cambrian
<i>Datasets & Resources</i>	
AFDB	AlphaFold Protein Structure Database
UR50	UniRef50 Protein Sequence Cluster
<i>**Biological terminology**</i>	
GO	Gene Ontology

B Reproducibility

Our implementations are based on widely adopted architectures, pretraining strategies, and downstream evaluation pipelines for protein modeling. The code is available at <https://github.com/Trust-App-AI-Lab/protap>. To ensure reproducibility, we provide detailed descriptions of the pretraining objectives in Section 3.2, along with the corresponding training configurations in Appendix G.2. Hyperparameters for all models, including learning rate schedules, batch sizes, and optimization settings, are explicitly reported in Section 5 and Appendix G.2. The datasets used for both pretraining and downstream evaluation are publicly available at <https://huggingface.co/datasets/findshuo/Protap>, and we specify their sources in Tab. 1 (b), and provide more details in Appendix F. The exact evaluation metrics are specified in Section Appendix F. These details, combined with the systematic comparison across architectures and strategies presented in Tab. 2 and Fig. 4, allow independent researchers to reproduce our results based on the manuscript alone.

C Comparison of benchmark coverage for protein modeling

We compare across three dimensions: applications (specialized vs. general), pretraining tasks, and model architectures (domain-specific vs. general). Comparisons with ProteinGym and ProteinBench are not included because their focuses differ from Protap.

ProteinGym [47] primarily targets mutation effect prediction with task-specific models. ProteinBench [70] emphasizes generative design tasks, e.g., backbone design and sequence-structure co-design, which are currently beyond Protap’s scope. Detailed objective coverage of benchmarks is provided in Tab.5.

D Supplemental Experiments and Observations

D.1 Descriptions and Categorization of Domain-Specific Models

The primary distinction between domain models and general models lies in their task-specific design. Domain models are tailored for particular tasks by enabling interaction between representations of different components and incorporating biochemical priors to enhance the encoder. In addition, domain models also leverage knowledge from other biochemical databases to preprocess the data, enabling the extraction of task-relevant key regions. Below, we summarize the characteristics of each domain model in relation to its respective tasks. Detailed task descriptions and model architectures are found in Appendix F and Appendix H.

Table 8: Domain Model Categorization

Category	Model
Biochemical Prior Enhancement	UniZyme, CLIPZyme, KDBNet, DeepFRI
Cross-Component Interaction	ET-PROTACs, DeepPROTACs
Hybrid	DPFunc, MONN

Enzyme-Catalyzed Protein Cleavage Site Prediction (PCS)

- **UniZyme.** UniZyme [31] not only incorporates pretraining for enzyme active site prediction but also introduces energetic frustration, an intrinsic biophysical phenomenon that directly reflects active site properties and catalytic mechanisms. The integration of such biochemical priors enhances the generalization capability of the enzyme encoder.
- **ClipZyme.** ClipZyme [41] formulates enzyme function prediction as a reaction-centric retrieval task, aligning enzyme representations with chemical reaction embeddings in a shared latent space. By explicitly modeling atom-mapped reaction graphs and constructing pseudo-transition states, the framework integrates reaction mechanism information that is specific to enzymatic catalysis.

Targeted Protein Degradation by Proteolysis-Targeting Chimeras (PRAOTACs)

- **DeepPROTACs.** DeepPROTACs [32] circumvent explicit modeling of the ternary complex by encoding different components of the Target protein-PROTAC-E3 ligase system using separate neural network modules.
- **ET-PROTACs.** ET-PROTACs [8] utilizes a cross-modal strategy and ternary attention mechanism, the model fully accounts for the cross-talk between PROTACs, target proteins, and E3 ligases, enabling more accurate modeling of ternary complex interactions.

Protein-Ligand Interactions (PLI)

Table 5: Comparison of benchmark coverage for protein modeling. ♣ indicates the presence of this dimension, while ○ denotes its absence.

		Protap (Ours)	PEER [68]	ProteinWorkshop [26]	TAPE [50]	ProteinGLUE [9]
Specialized Applications	Enzyme-catalyzed protein cleavage site prediction	♣	○	○	○	○
	Targeted protein degradation by Proteolysis-targeting chimeras	♣	○	○	○	○
	Protein–ligand interactions	♣	♣	○	○	♣
General Applications	Function prediction	♣	♣	♣	○	○
	Mutation effect prediction	♣	♣	○	♣	○
Pretraining Tasks	Masked language modeling	♣	○	♣	♣	♣
	Multi-view contrastive learning	♣	○	○	○	○
	Protein family prediction	♣	○	○	○	○
General Architectures	Protein language models	♣	♣	○	♣	♣
	Geometric GNNs	♣	○	♣	○	○
	Sequence-structure hybrid models	♣	○	○	○	○
Domain-specific Architectures	Protein function models	♣	○	○	○	○
	Enzyme domain models	♣	○	○	○	○
	Ternary complexes models	♣	○	○	○	○

Table 6: Performance comparison across model architectures under different training strategies with full parameter fine-tuning.

Model	PCS		PROTACs		PLI	
	C14.005		PROTACDB		Davis	
	AUC(%)↑	AUPR(%)↑	Acc(%)↑	AUC(%)↑	MSE↓	Pear(%)↑
EGNN w/MLM	95.36 ± 0.06	19.23 ± 0.31	79.03 ± 0.61	88.50 ± 0.37	0.461 ± 0.010	57.56 ± 1.18
EGNN w/MVCL	94.80 ± 0.00	19.61 ± 1.16	76.89 ± 2.50	88.81 ± 0.50	0.484 ± 0.031	56.18 ± 0.12
EGNN w/PFP	95.09 ± 0.41	27.95 ± 0.99	79.01 ± 0.55	87.65 ± 0.33	0.523 ± 0.036	55.44 ± 2.72
SE(3) Trans w/MLM	67.65 ± 1.31	0.55 ± 0.03	77.54 ± 0.06	87.08 ± 1.79	0.681 ± 0.109	43.20 ± 4.63
SE(3) Trans w/MVCL	44.01 ± 0.72	0.20 ± 0.00	75.59 ± 2.54	83.70 ± 0.04	1.110 ± 0.074	34.34 ± 4.76
SE(3) Trans w/PFP	69.27 ± 2.55	0.81 ± 0.17	77.60 ± 0.39	87.06 ± 0.66	0.536 ± 0.047	47.94 ± 3.51
ProtBERT w/MLM	95.45 ± 0.10	9.37 ± 0.62	77.09 ± 0.36	85.83 ± 0.73	0.511 ± 0.011	49.81 ± 1.32
ProtBERT w/MVCL	95.78 ± 0.21	28.51 ± 0.06	73.58 ± 0.13	83.40 ± 0.33	0.511 ± 0.008	50.25 ± 1.76
ProtBERT w/PFP	64.25 ± 0.35	0.36 ± 0.00	78.79 ± 0.85	87.41 ± 1.00	0.529 ± 0.018	49.99 ± 1.77
GVP w/MLM	89.09 ± 0.00	11.76 ± 0.01	72.54 ± 0.06	79.03 ± 0.01	0.438 ± 0.013	47.28 ± 0.00
GVP w/MVCL	88.68 ± 0.00	10.96 ± 0.01	71.45 ± 0.42	78.19 ± 0.13	0.423 ± 0.011	59.31 ± 0.00
GVP w/PFP	71.83 ± 0.01	1.50 ± 0.00	72.72 ± 0.36	79.94 ± 0.58	0.431 ± 0.002	59.04 ± 0.00
D-Trans w/MLM	94.40 ± 1.13	29.93 ± 0.09	74.46 ± 0.78	81.44 ± 0.59	0.464 ± 0.023	55.79 ± 0.50
D-Trans w/MVCL	98.11 ± 0.28	36.50 ± 3.17	73.26 ± 0.18	81.25 ± 0.50	0.437 ± 0.002	59.91 ± 0.13
D-Trans w/PFP	96.65 ± 0.21	34.55 ± 2.53	73.50 ± 0.30	82.64 ± 0.05	0.441 ± 0.020	59.66 ± 0.75
ESM-2	93.10 ± 1.71	55.09 ± 0.22	81.25 ± 1.44	88.17 ± 1.10	0.416 ± 0.011	59.59 ± 0.35
ESM-C	94.42 ± 0.10	35.25 ± 2.48	79.81 ± 0.36	86.65 ± 0.37	0.461 ± 0.00	53.35 ± 0.84
SaProt	94.75 ± 0.00	57.35 ± 0.01	81.43 ± 0.90	87.16 ± 0.13	0.423 ± 0.008	58.81 ± 0.02

- **KDBNet.** KDBNet [37] does not model the entire protein, instead, it defines the binding pocket based on prior knowledge from the KLIFS database. In modeling kinases, it incorporates both

geometric and evolutionary features, including backbone torsion angles and embeddings derived from the ESM language model.

- **MONN.** MONN [34] is a multi-objective neural network designed to simultaneously predict non-covalent interactions and binding

Table 7: Performance comparison across model architectures under different fine-tuning strategies.

Model	Pretrain objective	LR	PCS		PROTACs		PLI	
			C14.005		PROTACDB		Davis	
			AUC(%) \uparrow	AUPR(%) \uparrow	Acc(%) \uparrow	AUC(%) \uparrow	MSE \downarrow	Pear(%) \uparrow
EGNN	MLM	5e-6	95.49 \pm 0.44	32.61 \pm 1.09	78.98 \pm 2.09	87.02 \pm 1.53	0.497 \pm 0.042	52.80 \pm 1.84
		1e-6	95.47 \pm 0.23	34.34 \pm 0.70	80.01 \pm 1.92	88.96 \pm 1.24	0.485 \pm 0.018	56.50 \pm 3.65
		1e-7	95.41 \pm 0.37	28.14 \pm 1.19	79.11 \pm 1.69	87.77 \pm 1.16	0.506 \pm 0.051	52.92 \pm 3.82
	MVCL	5e-6	95.24 \pm 0.36	32.91 \pm 0.08	79.33 \pm 2.59	86.81 \pm 0.90	0.491 \pm 0.027	52.91 \pm 5.00
		1e-6	95.72 \pm 0.14	35.04 \pm 1.11	79.47 \pm 2.25	86.88 \pm 1.07	0.503 \pm 0.039	52.86 \pm 2.35
		1e-7	95.17 \pm 0.04	30.05 \pm 1.04	79.70 \pm 2.36	87.79 \pm 1.02	0.482 \pm 0.022	52.77 \pm 3.27
	PFP	5e-6	95.01 \pm 0.09	32.88 \pm 0.42	79.52 \pm 2.46	87.94 \pm 1.46	0.508 \pm 0.045	55.36 \pm 3.59
		1e-6	94.88 \pm 0.39	28.63 \pm 1.06	79.88 \pm 1.80	88.36 \pm 1.39	0.494 \pm 0.033	56.39 \pm 3.48
		1e-7	94.87 \pm 0.34	32.69 \pm 0.10	78.87 \pm 2.51	87.13 \pm 1.02	0.499 \pm 0.015	53.31 \pm 2.46
D-Trans	MLM	5e-6	98.11 \pm 0.00	63.50 \pm 0.18	77.76 \pm 2.55	85.15 \pm 1.42	0.450 \pm 0.040	59.59 \pm 0.91
		1e-6	97.88 \pm 0.07	60.12 \pm 0.32	76.08 \pm 1.19	83.46 \pm 0.64	0.465 \pm 0.034	58.07 \pm 0.53
		1e-7	97.76 \pm 0.09	57.79 \pm 0.87	74.88 \pm 0.85	82.46 \pm 0.82	0.467 \pm 0.022	56.71 \pm 0.14
	MVCL	5e-6	96.99 \pm 0.06	72.43 \pm 0.47	72.12 \pm 4.08	84.09 \pm 0.88	0.670 \pm 0.045	57.31 \pm 0.53
		1e-6	97.27 \pm 0.07	72.56 \pm 0.04	74.70 \pm 1.44	82.29 \pm 0.21	0.549 \pm 0.032	55.51 \pm 0.29
		1e-7	97.32 \pm 0.07	71.68 \pm 0.04	74.22 \pm 1.44	82.02 \pm 0.25	0.514 \pm 0.026	64.59 \pm 0.64
	PFP	5e-6	96.93 \pm 0.05	67.96 \pm 0.25	77.46 \pm 0.76	85.53 \pm 0.61	0.425 \pm 0.029	58.95 \pm 2.09
		1e-6	97.17 \pm 0.03	65.49 \pm 0.64	75.00 \pm 0.51	83.69 \pm 0.51	0.435 \pm 0.031	57.41 \pm 2.27
		1e-7	97.29 \pm 0.01	63.70 \pm 1.21	74.40 \pm 0.51	83.28 \pm 0.47	0.443 \pm 0.028	56.36 \pm 2.10
ProtBERT	MLM	5e-6	95.80 \pm 0.02	32.37 \pm 0.11	76.95 \pm 2.35	84.53 \pm 1.31	0.530 \pm 0.017	54.84 \pm 1.84
		1e-6	95.50 \pm 0.14	22.63 \pm 0.48	80.21 \pm 2.41	86.84 \pm 1.39	0.519 \pm 0.034	53.99 \pm 1.21
		1e-7	95.46 \pm 0.24	15.27 \pm 0.56	79.72 \pm 1.92	85.10 \pm 1.37	0.554 \pm 0.021	53.04 \pm 1.75
	MVCL	5e-6	95.74 \pm 0.21	23.83 \pm 0.14	78.05 \pm 1.21	84.83 \pm 1.88	0.546 \pm 0.035	55.28 \pm 1.91
		1e-6	95.25 \pm 0.20	33.23 \pm 0.53	80.42 \pm 1.59	85.53 \pm 1.45	0.534 \pm 0.026	55.73 \pm 1.29
		1e-7	95.05 \pm 0.09	33.25 \pm 0.65	79.43 \pm 1.55	86.98 \pm 1.68	0.547 \pm 0.035	55.78 \pm 1.63
	PFP	5e-6	64.52 \pm 0.44	4.54 \pm 0.80	78.35 \pm 1.89	84.69 \pm 1.39	0.527 \pm 0.034	52.34 \pm 1.62
		1e-6	63.88 \pm 0.25	6.41 \pm 0.60	77.85 \pm 1.82	88.00 \pm 0.97	0.553 \pm 0.033	53.82 \pm 1.77
		1e-7	64.24 \pm 0.38	0.41 \pm 0.60	78.94 \pm 2.72	86.56 \pm 1.35	0.549 \pm 0.037	51.36 \pm 1.29
ESM-2	MLM	5e-6	94.77 \pm 0.12	28.30 \pm 0.44	82.09 \pm 2.21	89.96 \pm 1.49	0.404 \pm 0.010	61.04 \pm 0.03
		1e-6	96.25 \pm 0.11	32.35 \pm 0.37	81.37 \pm 1.19	89.31 \pm 1.60	0.404 \pm 0.010	61.03 \pm 0.04
		1e-7	98.16 \pm 0.03	38.14 \pm 0.38	81.25 \pm 1.19	88.99 \pm 1.59	0.405 \pm 0.011	61.01 \pm 0.02

affinity between compounds and proteins, without relying on structural information.

Protein Function Annotation Prediction (PFA)

- **DeepFRI.** DeepFRI [20] employs graph convolutional networks (GCNs) [28] to process protein contact maps and integrates representations pretrained on Pfam sequences.
- **DPFunc.** DPFunc [64] identifies key functional regions within protein structures and precisely predicts their associated biological functions by leveraging protein domain information.

D.2 Detail of Friedman–Nemenyi Tests for Pretraining Objectives

We compare three pretraining strategies (MLM, MVCL, PFP) using rank-based Friedman tests and Nemenyi post-hoc analyses across five backbones (EGNN, SE(3)-Trans, GVP, ProtBERT, D-Trans). To avoid redundancy across correlated metrics, we select one representative metric per task: AUC for PCS (C14.005) and PROTACs,

Pearson correlation for PLI, and F_{\max} for PFA, yielding $5 \times 4 = 20$ evaluation blocks. (MTP is excluded since it is only applicable to MLM). Lower average rank is better.

D.3 Additional Observations

To provide a more comprehensive evaluation, we perform full parameter fine-tuning of the pretrained models on three downstream tasks, namely PCS, PROTACs, and PLI, with all encoder parameters updated during training. The corresponding results are presented in the Tab. 6. Generally, performing full-parameter fine-tuning on the entire model with a larger learning rate (1×10^{-4}) generally leads to slightly lower performance compared to the encoder-freezing setting. This suggests that overly aggressive full fine-tuning is less stable and often degrades ranking and regression metrics across specialized applications. This further reinforces our observation in RQ1: the effective use of pretrained models requires not only preserving pretrained knowledge but also providing the necessary representation adaptation capacity.

Table 9: Statistical comparison of pretraining objectives.

Scope	Metric	n	χ^2	p -value	W	CD	Rank _{MLM}	Rank _{MVCL}	Rank _{PPF}
Overall	Mixed	20	6.10	0.047	0.153	0.741	1.75	2.30	1.95
PCS	AUC \uparrow	5	1.20	0.549	0.120	1.480	1.80	2.00	2.20
PROTACs	AUC \uparrow	5	2.80	0.247	0.280	1.480	2.60	2.20	1.20
PLI	Pearson \uparrow	5	0.40	0.819	0.040	1.480	1.80	2.20	2.00
PFA	F_{\max} \uparrow	5	6.40	0.041	0.640	1.480	2.00	2.80	1.20

Notes. χ^2 is the Friedman statistic and W is Kendall’s coefficient of concordance ($W = \chi^2 / (n(k-1))$), with $k=3$ strategies). CD denotes the Nemenyi critical difference at $\alpha=0.05$; pairwise average-rank gaps exceeding CD are significant. For PFA, $|\Delta R| = |1.20 - 2.80| = 1.60 > CD = 1.48$ (PPF vs. MVCL). For Overall, the largest rank gap is $|1.75 - 2.30| = 0.55 < 0.741$, hence no pairwise difference is significant.

Table 10: Results on KIBA Dataset.

	EGNN	EGNN w/PPF	SE(3) Trans	SE(3) Trans w/MVCL	ProtBERT	ProtBERT w/MVCL	ESM-2
MSE \downarrow	0.434 \pm 0.007	0.396 \pm 0.006	0.442 \pm 0.034	0.473 \pm 0.026	0.471 \pm 0.005	0.393 \pm 0.001	0.454 \pm 0.004
Pear(%) \uparrow	65.09 \pm 0.68	65.27 \pm 0.15	63.19 \pm 1.15	58.57 \pm 1.84	60.89 \pm 3.66	65.10 \pm 0.76	58.14 \pm 0.01

E Preliminaries

E.1 Protein Data

Proteins obtained through high-throughput sequencing are typically represented as sequences. However, using laboratory techniques such as X-ray crystallography, electron microscopy, XFEL, and nuclear magnetic resonance, the 3D structures of proteins can be elucidated. Unlike Computer Vision and Natural Language Processing, proteins can be characterized using various descriptions, such as 1D sequences, 2D graphs, and 3D structures.

Sequence. The most common representation is the amino acid sequence, typically in FASTA format using single-letter codes. Sequence-based models, originally RNNs and CNNs, are now dominated by Transformers due to their superior long-range modeling. Large pre-trained models such as ESM-2 [35, 54], ProteinBERT [6], and ProtTrans [16] capture biochemical properties and evolutionary relationships, with structural information implicitly encoded in their learned representations.

2D Graph. Proteins can also be described as molecular graphs, with residues as nodes and chemical or spatial relationships as edges. 2D graphs capture connectivity and topological features but lack explicit spatial details. Contact maps and models like GraphFormer [71] encode residue-residue proximity or graph connectivity into the attention mechanism, partially reflecting structural information.

3D Structure. Many methods have been developed for modeling the 3D structures of proteins. 3D CNNs employ convolutional neural networks to extract local spatial features of proteins. Graph neural networks are widely used for representing protein and molecular structures, with examples including proteinMPNN [11], SE(3)-Transformer [17], GVP [27], and GearNet [74]. GearNet applies contrastive learning for the pre-training of protein structures. Additionally, Transformer-M [36] incorporates 3D information through distance matrices, enabling transformers to represent protein 3D structures while maintaining invariance. More recently, some works have begun to include protein surface information in modeling; for

instance, ProteinINR [30] integrates sequence, 3D structure, and surface information to enhance protein representations.

E.2 Terminology

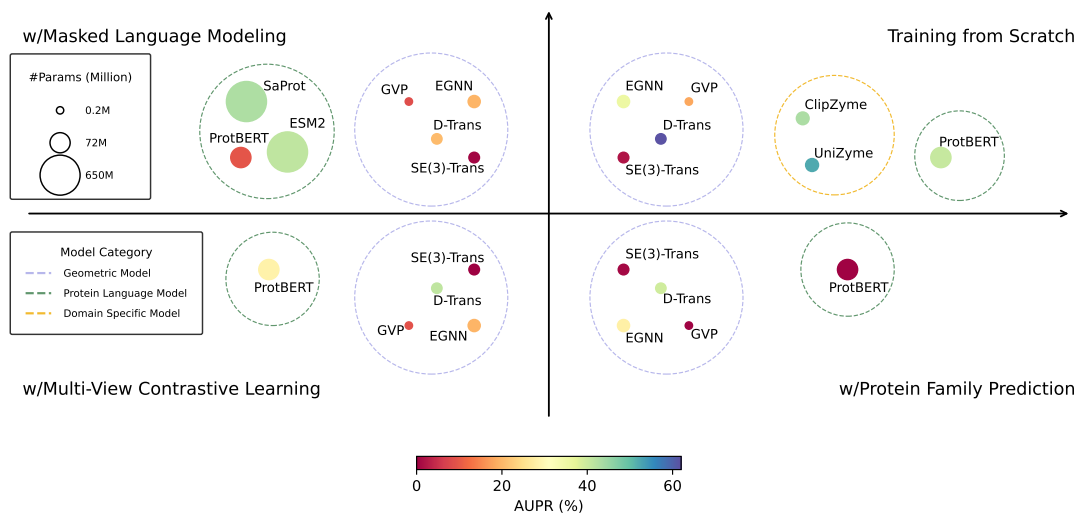
This section provides detailed definitions of the professional terms used in the paper.

Protein Family. A protein family is a group of evolutionarily related proteins that typically share similar amino acid sequences, three-dimensional structures, and biological functions. Most members of a protein family are encoded by genes from a corresponding gene family, where each gene-protein pair has a one-to-one relationship. To date, more than 60,000 protein families have been identified, though exact numbers vary depending on the criteria and classification methods used.

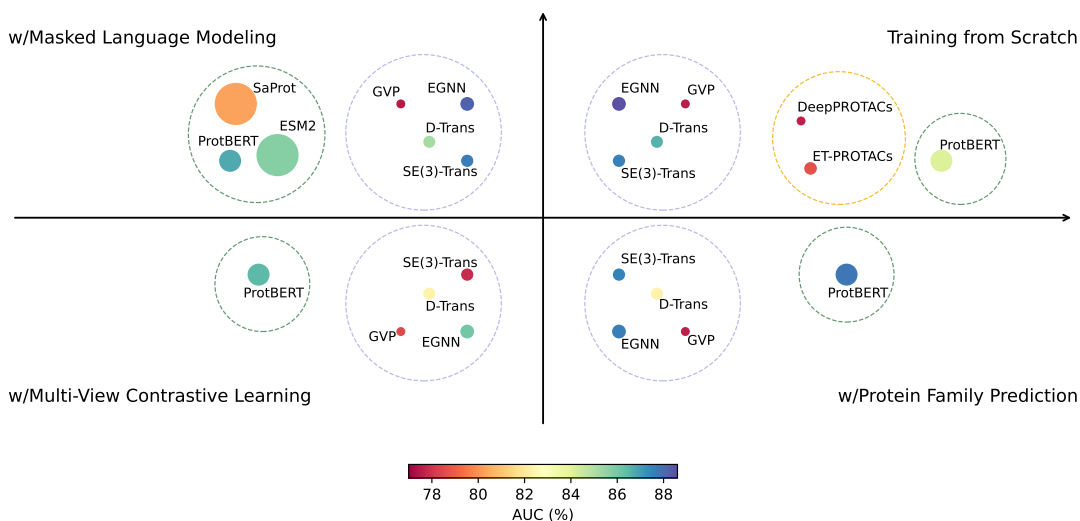
Enzyme-catalyzed Protein Cleavage. Proteolytic enzymes first recognize short sequences or structural motifs within a substrate protein and then hydrolyze the peptide bond at the corresponding cleavage site, thereby fragmenting the polypeptide chain. This tightly regulated process governs protein maturation, turnover, and signaling, and its accurate in-silico prediction assists enzyme engineering and therapeutic target identification.

Proteolysis-Targeting Chimeras (PROTACs). A PROTAC is a heterobifunctional small molecule comprising (i) a warhead that binds the target (disease-relevant) protein, (ii) a chemical linker, and (iii) an E3-ligase-recruiting ligand. By simultaneously engaging the target protein and an E3 ubiquitin ligase, a PROTAC forms a ternary complex that drives poly-ubiquitination of the target, leading to its proteasomal degradation. Because PROTACs act catalytically and do not rely on classical active-site inhibition, they can eliminate previously “undruggable” proteins and often function at lower doses than conventional inhibitors.

Protein-Ligand Binding Affinity. Protein–ligand binding denotes the selective, high-affinity association between a protein and a small-molecule ligand to form a stable complex. Binding strength is quantified by the change in Gibbs free energy (ΔG) or related measures such as the dissociation constant (K_d); a more negative



(a) Comparisons between general and domain models on protein cleavage site prediction (PCS).



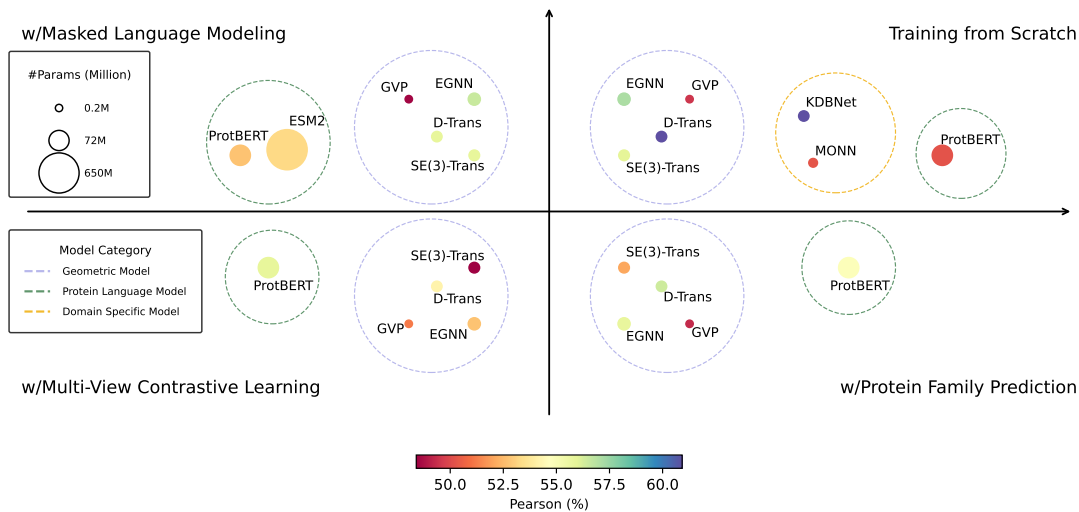
(b) Comparisons between general and domain models on targeted protein degradation by proteolysis-targeting chimeras (PROTACs).

Figure 7: Visualization of model size and performance across two specialized tasks: (a) PCS and (b) PROTACs. Each point represents a model, with size indicating parameter count and color intensity reflecting task performance. Each point represents a model, with its size corresponding to the number of parameters, ranging from 2M for GVP to 650M for ESM. Larger points indicate larger models. The color intensity of each point indicates performance, with darker shades representing stronger results. The dashed circular boundaries group models by category: models incorporating geometric information in **color**, protein language models in **color**, and domain-specific models in **color**.

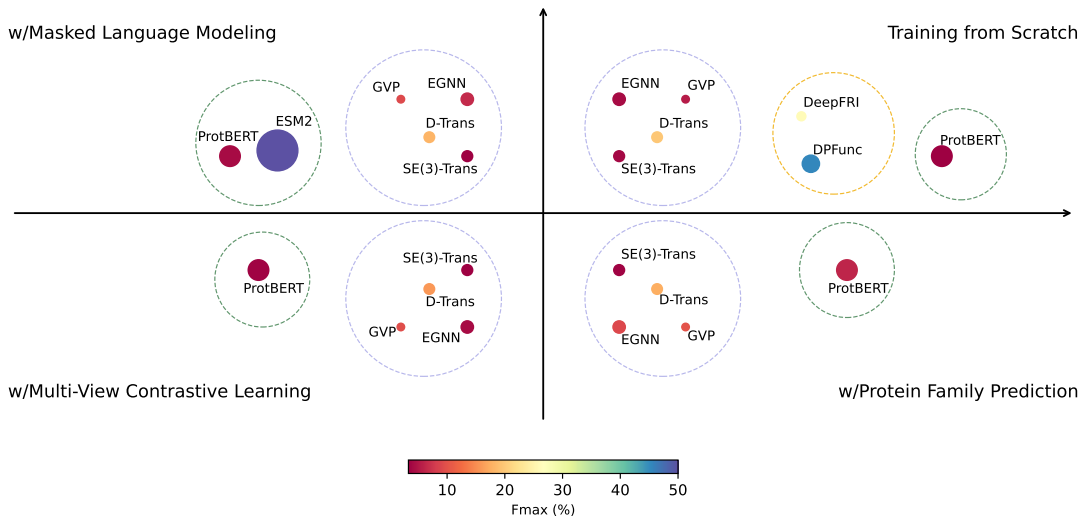
ΔG (or lower K_d) reflects stronger affinity. Reliable computational estimation of binding affinity accelerates virtual screening and lead optimization in drug discovery by prioritizing ligands most likely to bind their target proteins.

Gene Ontology (GO). Gene Ontology is a standardized vocabulary used to describe the functions of genes and proteins in a consistent and structured way. It provides a common language that allows researchers across different species and databases to describe what a gene product does, where it does it, and what biological processes it is involved in. GO is organized into three main categories, known as ontologies: (i) Biological Process (BP), which describes the broader

biological goals that a gene or protein contributes to. (ii) Molecular Function (MF), which defines the specific biochemical activity of the gene product. (iii) Cellular Component (CC), which indicates the location within the cell where the gene product is active. Each GO term is assigned a unique identifier, e.g., GO: 0003677 for “DNA binding”.



(a) Comparisons between general and domain models on Protein-Ligand Interaction (PLI).



(b) Comparisons between general and domain models on protein function prediction (PFA).

Figure 8: Visualization of model size and performance across two general tasks: (a) PLI and (b) PFA. Each point represents a model, with size indicating parameter count and color intensity reflecting task performance.

F Detail of Downstream Application and Dataset

F.1 Enzyme-Catalyzed Protein Cleavage Site Prediction

Task Definition. Cleavage site prediction is formulated as a large-scale, imbalanced, residue-level binary classification problem. Let P_s denote a substrate protein of length $|R|$, and for each residue r_j ($j = 1, \dots, |R|$), let $x_j \in \mathbb{R}^d$ be its feature vector. The objective is to learn a function

$$f: \mathbb{R}^d \rightarrow \{0, 1\}$$

that outputs 1 if r_j is a cleavage site under catalysis by a given enzyme, and 0 otherwise. Formally, each substrate P_s is associated

with a label vector $Y \in \{0, 1\}^{|R|}$, where $Y_j = 1$ indicates cleavage at residue j . Training proceeds over residue-level examples $\{(x_j, Y_j)\}$ sampled from annotated cleavage datasets, enabling model generalization to varied substrate contexts.

Settings. For all pretrained models, we retain the same architectural hyperparameters as used during pretraining. During downstream training, we use a unified configuration across all models: the number of training epochs is set to 50, the learning rate to 1×10^{-4} , and the batch size to 24. A cosine annealing scheduler is employed to adjust the learning rate over time. To ensure robustness and reproducibility, we fix a set of five random seeds $\{42, 128, 256, 512, 1024\}$. For each model, we report the mean and standard deviation of

its performance across these five runs. All experiments were conducted using 8 NVIDIA L40 GPUs. The average training time varied depending on the model size and task complexity, ranging from approximately 15 minutes to 5 hours.

Metric. The evaluation of enzyme-catalyzed protein cleavage site prediction is framed as a residue-level binary classification task under substantial class imbalance. Accordingly, the area under the receiver operating characteristic curve (AUC) and the area under the precision-recall curve (AUPR) are used as primary evaluation metrics. AUC quantifies the trade-off between true positive rate (TPR) and false positive rate (FPR) across various classification thresholds, offering a global view of discriminative ability. However, due to the rarity of cleavage sites, AUPR is considered more informative, as it emphasizes the precision-recall behavior specific to the minority class. In particular, AUPR reflects the expected precision over all recall levels, which is critical for the reliable detection of enzymatic cleavage sites.

Dataset. The detailed information of the dataset is as follows:

- **Data Source.** The original data are from the MEROPS [51] database. This dataset has a public website, available at the following address: <http://cadd.zju.edu.cn/protacdb/>
- **Pre-process.**
 - Prior studies [51] have shown that slight sequence variations among enzymes within the same MEROPS category are negligible. As a result, we generalize the hydrolysis data from a specific substrate-enzyme interaction to all enzymes in that category. This allowed us to augment our dataset by linking each substrate not only to its originally annotated enzyme but also to other enzymes classified in the same MEROPS group. Finally, we selected two enzyme families, C14.003 and M10.003, for evaluation.
 - We performed quality control on the raw data by filtering out entries with hydrolysis sites exceeding the maximum sequence length.
 - We converted the structural data of proteins in the dataset into a dictionary format and stored it in a `.pickle` file. The fields are as follows:

```
{
  "Q5QJ38": {
    "name": "Q5QJ38",
    "seq": "MPQLLRNVLCVIETFHKYASEDSNGAT..",
    "coords": [[[-0.43, 25.50, -8.24], ..], ..],
    "cleave_site": [136]
  }
}
```

- **Data Format.** The sequence and structure of substrate proteins are stored in a `.pickle` file. The hydrolysis site information of substrate proteins is stored in a `.pickle` file as follows. It is worth noting that the hydrolysis site positions are 1-based indexed.

```
{
  "P31001_MER0000622": [110, 263],
  "000232_MER0000622": [276, 334, 19],
  ...
}
```

- **Data Statistics.** The statistics of the dataset after preprocessing are summarized in Table 11. The training and test sets were

split based on sequence similarity, ensuring that the sequence similarity between the test and training sets is below 60%.

Table 11: Statistics of the dataset after preprocessing.

Enzyme Family	#Train	#Test	Sites (Train)	Sites (Test)
C14.005	468	117	656	159
M10.003	375	92	953	157

- **Usage.** This dataset is used for a residue-level binary classification task. The goal is to predict the hydrolysis sites of a protein by a given enzyme family, based on its sequence or structure.
- **License.** We release a preprocessed version of the dataset under the MIT License. The original MEROPS database is provided under the terms of the GNU Library General Public License and is available at: <https://www.ebi.ac.uk/merops/about/availability.shtml>.

F.2 Targeted Protein Degradation by Proteolysis-Targeting Chimeras

Task Definition. This task is typically formulated as a binary classification problem. Given a PROTAC candidate and its corresponding POI and recruited E3 ligase, the goal is to predict whether the induced ternary complex will successfully trigger degradation. Formally, let the PROTAC molecule be decomposed into three modular components: warhead w , linker l , and E3-ligand el . Along with the protein of interest p and the E3 ligase eg , each component is processed through dedicated neural encoders:

$$\mathbf{h}_p = f_p(p), \quad \mathbf{h}_w = f_w(w), \quad \mathbf{h}_l = f_l(l), \quad \mathbf{h}_{el} = f_{el}(el), \quad \mathbf{h}_{eg} = f_{eg}(eg)$$

The resulting latent representations are concatenated to form a joint embedding that captures the structural and biochemical context of the ternary complex:

$$\mathbf{h}_{\text{concat}} = \text{concat}(\mathbf{h}_p, \mathbf{h}_w, \mathbf{h}_l, \mathbf{h}_{el}, \mathbf{h}_{eg})$$

This composite feature vector is passed through a multi-layer perceptron (MLP) with two fully connected layers to output the degradation prediction score:

$$\hat{y} = \sigma(\text{MLP}(\mathbf{h}_{\text{concat}})) \in [0, 1]$$

where \hat{y} denotes the predicted probability of successful POI degradation. The model is trained using binary cross-entropy loss, with ground truth labels indicating degradation activity.

Settings. For this task, we retain the same architectural hyperparameter configuration as used during pretraining. To encode SMILES representations, we adopt the GVP [27] architecture with a node dimensionality of 128, an edge dimensionality of 32, and a total of 3 layers. Models are trained for 50 epochs with a learning rate of $5e-4$, a batch size of 24, and the Adam optimizer. We report the mean and standard deviation of performance across a fixed set of random seeds. All experiments are conducted on NVIDIA L40 GPUs, with per-run training time ranging from approximately 20 minutes to 6 hours, depending on the model and task complexity.

Metrics. The evaluation of PROTAC-induced protein degradation prediction is framed as a binary classification task. Accordingly, we adopt two widely used classification metrics: Accuracy measures

the proportion of correct predictions among all samples, providing a straightforward indication of overall model performance. Area Under the Receiver Operating Characteristic Curve (AUC) quantifies the model’s ability to distinguish degraders from non-degraders across varying decision thresholds.

Dataset. The detailed information of the dataset is as follows:

- **Data Source.** The original data was collected from the PROTAC-DB [19]. This dataset has a public website, available at the following address: <http://cadd.zju.edu.cn/protacdb/>
- **Pre-process.**
 - Following the processing strategy proposed by ET-PROTACs [8], we assign a degradation label to each triplet in the dataset. Specifically, we first examine whether a PROTAC entry contains DC_{50} measurements. If available, entries with DC_{50} values below 1000 nM are labeled as active, while those equal to or above 1000 nM are labeled as inactive. For entries lacking DC_{50} data, we instead inspect the reported degradation percentage of the target protein. If available, samples with degradation rates of at least 70% are considered active, and those below 70% are labeled as inactive. In cases where neither DC_{50} nor degradation percentage is reported, we fall back to IC_{50} values. Similarly, entries with IC_{50} below 1000 nM are labeled as active, and those above or equal to this threshold are labeled as inactive.
 - For the target protein and E3 ligase, we retained only the entries with available structures in the AFDB. We filtered out the target proteins with the following UniProt IDs: P36969, P03436, P0DTD1, Q12830, and G0R7E2. The structural data of the target proteins and E3 ligases are obtained from AFDB. Following the approach in [25], we further convert the format into a dictionary and store it in a .json file. The fields are as follows:

```
[
  "Q8IWW7": {
    "seq": "MADEEAGGTERMEISAE L P Q T P Q R L A S W W . . ",
    "coord": [[ [ 21.99, 68.31, -49.90 ], . . ], . . ]
  }
  ..
]
```

 For each structure, coord is a nested list of shape $(N \times 4 \times 3)$, representing the 3D coordinates of the backbone atoms N, Ca, C, and O for each residue in order, and N is the length of the amino acid sequence.
 - For the warhead, linker, and E3-ligand, we use their SMILES strings to generate 20 conformers with RDKit’s ETKDGv3 method. The conformers are optimized using a force field, and the lowest-energy conformer is selected. The final structure is saved in an SDF file.
- **Data Format.** The protein data, including the name, sequence, and coordinates, is stored in .json format. The structures of the warhead, linker, and E3-ligand are stored in SDF files. The label data is saved in a .txt file with the following format. The content below shows only key fields; for the complete list of fields, please refer to the full file.

```
uniprot  e3_ligase  linker  warhead  e3_ligand  label
Q00987  Q96SW2  linker_2  warhead_7  e3_ligand_7  1
Q00987  Q96SW2  linker_2  warhead_7  e3_ligand_16  1
```

```
P10275  P40337  linker_13  warhead_27  e3_ligand_27  0
P10275  P40337  linker_33  warhead_27  e3_ligand_27  0
```

- **Data Statistics.** The number of each component in the dataset is summarized in Table 12. The dataset was randomly split into a training set and a test set, with 80% used for training and 20% for testing.

Table 12: Statistics of PROTACs dataset components.

Target Protein	E3-Ligase	Warhead	Linker	E3-Ligand	Label: 1	Label: 0
154	10	552	1,534	131	2,244	1,878

- **Usage.** Based on the preprocessed reaction labels, this dataset is used for a binary classification task, where the goal is to predict the targeted degradation effect of PROTACs given the information of the target protein, E3 ligase, and the PROTACs.
- **License.** We release a preprocessed version of the dataset under the MIT License. Please refer to the usage license of the original data at: <http://cadd.zju.edu.cn/protacdb/downloads>, and follow the original authors’ terms of use.

F.3 Protein–Ligand Interactions

Task Definition. Protein-ligand binding is the process by which proteins or various small molecules interact with high specificity and affinity to form a particular complex. A thorough understanding of the mechanisms underlying protein-ligand interactions is a prerequisite for gaining in-depth insights into protein function. The goal of rational drug design is to leverage structural data and knowledge of protein-ligand binding mechanisms to optimize the process of discovering new drugs. The driving force for protein-ligand binding arises from a combination of interactions and energy exchanges among proteins, ligands, water molecules, and buffering ions. Because the extent of protein-ligand binding is determined by the magnitude of negative ΔG , ΔG can be considered to determine the stability of any given protein-ligand complex, or equivalently, the binding affinity of a ligand for a given receptor. Experimentally measuring protein-ligand binding affinity is both time-consuming and complex, making it impractical to rely solely on experimental approaches for drug discovery from large compound libraries. In computational medicinal chemistry, predicting ligand binding affinity remains an open challenge. Existing deep learning methods attempt to directly predict binding affinity using affinity data from databases such as PDBBind.

From a machine learning perspective, protein-ligand affinity prediction is formulated as a regression problem, where the goal is to learn a function

$$f : \mathbb{R}^d \rightarrow \mathbb{R}$$

that maps the given input features X_i (e.g., protein structural or sequence data, ligand chemical descriptors, etc.) to a continuous value $y_i \in \mathbb{R}$, representing the quantitative binding affinity. Concretely, each protein-ligand pair (P_i, l_i) is associated with a feature vector $X_i \in \mathbb{R}^d$ and an affinity value y_i . The learning objective is to minimize the discrepancy between the predicted affinity $\hat{y}_i = f(X_i)$ and the experimentally measured (or otherwise ground-truth) value y_i , typically via metrics such as root mean squared error (RMSE) or

mean absolute error (MAE). The function f can be learned using a training dataset

$$\{(X_i, y_i)\}_{i=1}^n,$$

and subsequently evaluated on unseen data to gauge its predictive performance and generalizability, ultimately utilized for drug screening.

Settings. For this task, we retain the same architectural hyperparameter configuration as used during pretraining. To encode SMILES representations, we adopt the GVP [27] architecture with a node dimensionality of 128, an edge dimensionality of 32, and a total of 3 layers. The maximum length of the pocket amino acid sequence is set to 85 residues, with shorter sequences padded and longer sequences truncated accordingly. Models are trained for 50 epochs with a learning rate of $5e-4$, a batch size of 48 or 96, and the Adam optimizer. We report the mean and standard deviation of performance across a fixed set of random seeds. All experiments are conducted on NVIDIA L40 GPUs, with per-run training times ranging from approximately 20 minutes to 5 hours, depending on the model and task complexity.

Metrics. To assess a model’s ability to predict binding affinity accurately, we adopt two complementary metrics: Mean Squared Error (MSE) and Pearson correlation coefficient. A lower MSE indicates more accurate regression of affinity values, while a higher Pearson coefficient reflects stronger linear correlation between predicted and true affinities. These metrics jointly capture both the precision and consistency of model predictions, providing a comprehensive evaluation of regression performance.

Dataset. The detailed information of the dataset is as follows:

- **Original Data Source.** The original data was collected from the KDBNet [37]. The data is stored at <https://www.dropbox.com/s/owc45bzbf05ix4/data.tar.gz>. Based on the existing DAVIS [12] and KIBA [59] datasets, the authors further extracted the binding pockets of proteins from protein-ligand complexes for use in modeling this task.

- **Preprocess.**

- In the DAVIS portion of the KDBNet dataset, the protein 6FDY . U contains missing coordinate values, which we filter out.
- Following the approach in [25], we convert the format of the protein structural data provided by the authors and store it as a dictionary in a JSON file:

```
[
  "4WSQ.B": {
    "uniprot_id": "Q2M2I8",
    "seq": "EVLAEGGFAIVFLCALKRMVCKREIQIM. .",
    "coord": [[[6.60, 16.25, 52.32], . .], . .]
  }
  ..
]
```

For each structure, coords is a nested list of shape $(N \times 4 \times 3)$, representing the 3D coordinates of the backbone atoms N, Ca, C, and O for each residue in order, and N is the length of the amino acid sequence.

- **Format.** The protein data, including the name, UniProt ID, sequence, and coordinates, is stored in .json format. The label data is saved in a .txt file with the following format:

```
drug    protein    Kd        y    protein_pdb
```

```
0    5291    AAK1    10000.0    5.0    4WSQ.B
1    5291    ABL1p    10000.0    5.0    3QRJ.B
2    5291    ABL2    10.0    7.99568    2XYN.C
```

The ligand data is stored in SDF format.

- **Statistics.** As shown in Table 13, DAVIS contains 226 proteins, 64 compounds, and 14,464 interaction pairs, while KIBA includes 160 proteins, 1,986 compounds, and 89,958 pairs. The dataset was randomly split into a training set and a test set, with 80% used for training and 20% for testing. These datasets vary in scale and compound diversity, providing a comprehensive benchmark for model evaluation.

Table 13: Statistics of protein–ligand datasets.

Dataset	Protein	Ligand	Pair
DAVIS	226	64	14,464
KIBA	160	1,986	89,958

- **Usage.** This dataset is used for a regression task, where the goal is to predict the binding affinity for each protein–ligand pair.
- **License.** We release a preprocessed version of the dataset under the MIT License. The original dataset, also licensed under the MIT License, is available at: <https://github.com/luoyunan/KDBNet/blob/main/LICENSE>.

F.4 Protein Function Annotation Prediction

Task Definition. From a computational standpoint, protein function prediction is inherently a large-scale, sparse, and imbalanced multi-label classification problem. The goal is to predict multiple output labels from the given input features X_i . Let the set of labels be

$$\mathcal{L} = \{\text{BP, MF, CC}\}$$

Thus, each protein P_i is associated with a label vector $Y_i \in \{0, 1\}^{|\mathcal{L}|}$, where $Y_i[j] = 1$ indicates that protein P_i is annotated with the j -th label, and $Y_i[j] = 0$ indicates it is not.

The goal is to learn a mapping function $f(X_i)$ to predict the label vector Y_i , i.e.:

$$f : \mathbb{R}^d \rightarrow \{0, 1\}^{|\mathcal{L}|}$$

This function can be learned using the training dataset $\{(X_i, Y_i)\}_{i=1}^n$.

Settings. For this task, to rigorously assess the model’s generalization ability, we included only those test sequences whose similarity to the training set was below 50%. we adopt the same architectural hyperparameter settings as used during pretraining to ensure consistency. Each model is trained for 50 epochs using the Adam optimizer with a learning rate of $5e-4$ and a batch size of 24. To ensure robustness, we report the average performance and standard deviation across a predefined set of random seeds. All training is conducted on NVIDIA L40 GPUs, with individual runs taking between 2 minutes and 10 hours, depending on the model architecture and task complexity.

Metrics. Given the inherent sparsity of function annotation labels, where each protein is typically associated with only a small subset of possible functions, we evaluate model performance using Fmax and AUPR (Area Under the Precision-Recall Curve). These metrics are particularly suited for imbalanced multilabel classification tasks, where a higher Fmax and AUPR indicate better predictive capability in accurately identifying relevant functional annotations.

Dataset. The detailed information of the dataset is as follows:

- **Data Source.** The original data are from DeepFRI [20](<https://github.com/flatironinstitute/DeepFRI>), and the corresponding structural data are collected by ProteinWorkshop [26](<https://zenodo.org/records/8282470/files/GeneOntology.tar.gz?download=1>).

- **Pre-process.**

- We performed quality control on the raw data by filtering out entries with missing coordinates or with all function labels equal to 0.
- Based on the label annotations and protein information provided in the original dataset, we unified each protein entry into a dictionary format containing its name, sequence, coordinates, and functional labels. The final data was saved in a .json file, with each entry structured as follows:

```
[
  {
    "name": "2P1Z-A",
    "seq": "SKKAELAEELVKELAVYVDLRRATLHARASR...",
    "coords": [[6.43, 51.38, 15.44], ..], ..],
    "molecular_function": [0, 0, ..1,..],
    "biological_process": [0, 0, ..0,..],
    "cellular_component": [0, 0, ..1,..]
  },
  ...
]
```

The fields `molecular_function`, `biological_process`, and `cellular_component` store one-hot encoded functional annotations. If you need Gene Ontology term IDs corresponding to the functional labels, please refer to the `label.tsv` file. The order of entries in this file strictly matches the position of each label in the one-hot vectors.

- **Data Format.** The protein name, sequence, coordinates, and functional labels are stored in a .json file. The corresponding Gene Ontology terms for the functional labels are provided in the `label.tsv` file.
- **Data Statistics.** Since *molecular function* defines the biological roles that a protein participates in, we restrict our functional prediction evaluation to *molecular function* only. The following Table 14 summarizes the label distribution across all proteins in the dataset. Label 1 refers to the total number of positive functional labels associated with proteins. Label 0 refers to the total number of functional labels not associated with the proteins.

Table 14: Statistics of positive and negative functional labels in the training and test sets.

Objective	#Train	#Test	Train		Test	
			Label: 1	Label: 0	Label: 1	Label: 0
Number	23,760	202	121,650	11,496,990	17,709	971,538

- **Usage.** This dataset is used for a multi-label classification task, where the goal is to predict the functional labels of each protein based on its sequence and structural information.

- **License.** We release a preprocessed version of the dataset under the MIT License. The original dataset is available under a BSD 3 license at <https://github.com/flatironinstitute/DeepFRI/blob/master/LICENSE>. And the protein structure data is released under the CC BY 4.0 license and is available at: <https://openreview.net/pdf?id=sTYuRVrdK3>

F.5 Mutation Effect Prediction for Protein Optimization

Task definition. The log-ratio between wild-type and mutant amino acid probabilities has been shown to be an effective estimator of mutational impact [46, 53]. In the zero-shot setting, we do not access any label information. Instead, we perform inference using a model pretrained with masked language modeling (MLM). The goal is to quantify the log-likelihood of protein variants under the background. The calculation is shown in the equation.

$$\sum_{t \in T} \log p(x_t = x_t^{mut} | S_{-t}) - \log p(x_t = x_t^{wt} | S_{-t})$$

where T is a set of positions where multiple mutations exist in the same sequence, and S is the wild-type sequence.

Settings. In the zero-shot setting, we do not use any label information, nor do we perform further training or fine-tuning. The prediction of mutation effects relies on the model’s estimated probabilities for the mutant and wild-type amino acids at the mutation site. Therefore, pretraining methods whose models do not expose logits are unsuitable for this zero-shot setting, and no additional domain-specific models are incorporated in this study. Other types of pretraining methods are not suitable for this zero-shot scenario, and no additional domain-specific models are introduced in this application.

Metrics. Due to the non-linear relationship between protein function and fitness, the Pearson correlation coefficient is a suitable metric for evaluating model performance. Another evaluation metric is AUC, which assesses the model’s ability to rank and discriminate between functionally neutral and deleterious mutations. During AUC calculation, `DMS_Score_Bin` is used as the ground-truth label (1 = positive, 0 = negative), while the model’s continuous prediction scores serve as the decision function.

Dataset. The detailed information of the dataset is as follows:

- **Data Source.** The dataset we used to evaluate in this benchmark is from ProteinGym [20](<https://proteingym.org/>)
- **Pre-process.** Structural data is predicted by OmegaFold [67], where the input sequences for structure prediction are the wild-type sequences. We removed samples for which OmegaFold failed to generate structural predictions due to excessive sequence length.
- **Data Format.** The DMS substitution data provided by ProteinGym is formatted as shown below. The first column contains the mutation information, using 1-based indexing. For example, F1I indicates that the first amino acid in the wild-type sequence, originally phenylalanine (F), is mutated to isoleucine (I).

mutant	mutated_sequence	DMS_score	DMS_score_bin
F1I	ITLIELMIVIAIVGILA..	-3.598	0
F1L	LTLIELMIVIAIVGILA..	-0.678	0
F1V	VTLIELMIVIAIVGILA..	1.299	1

F1S	STLIELMIVIAIVGILA..	-0.127	0
T2A	FALIELMIVIAIVGILA..	0.786	1

- **Data Statistics.** After preprocessing, the dataset contains 201 proteins and 2,413,913 mutations. The detailed statistics of the preprocessed dataset are shown in Table 15.

Table 15: Overall statistics of the ProteinGym DMS substitution dataset.

Objective	Proteins	Mutants
Number	201	2,413,913

- **Hosting.** The ProteinGym dataset is well-organized, and aside from adding structural information predicted by OmegaFold (while AlphaFold-predicted structures for DMS data are also available on the ProteinGym website), we did not perform any additional preprocessing. Therefore, we do not release a separate preprocessed version of the data.
- **Usage.** In the zero-shot setting, this evaluation involves no training process. Instead, it directly infers and quantifies the log-likelihood of protein variants under both sequence and structural context.
- **License.** The original dataset, ProteinGym, is available under a MIT license at <https://github.com/OATML-Markslab/ProteinGym/blob/main/LICENSE>.

G Pretrain Model Architecture and Experimental Setup

G.1 Model Architecture

This section details the models employed in this study.

Equivariant Graph Neural Networks (EGNN). EGNN [56] is designed to process graphs where each node is associated with both feature embeddings and spatial coordinates. EGNN preserves equivariance under Euclidean transformations (translation and rotation) and node permutations, making it well-suited for modeling molecular and protein structures.

Given a graph $\mathcal{G} = (\mathcal{V}, \mathcal{E})$, each node $v_i \in \mathcal{V}$ has a feature vector $\mathbf{h}_i \in \mathbb{R}^{d_h}$ and a coordinate $\mathbf{x}_i \in \mathbb{R}^n$. The Equivariant Graph Convolutional Layer (EGCL) updates node features and coordinates as follows:

$$\mathbf{m}_{ij} = \phi_e \left(\mathbf{h}_i^l, \mathbf{h}_j^l, \|\mathbf{x}_i - \mathbf{x}_j\|^2, a_{ij} \right), \quad (1)$$

$$\mathbf{x}_i^{l+1} = \mathbf{x}_i^l + C \sum_{j \neq i} (\mathbf{x}_i^l - \mathbf{x}_j^l) \cdot \phi_x(\mathbf{m}_{ij}), \quad (2)$$

$$\mathbf{m}_i = \sum_{j \neq i} \mathbf{m}_{ij}, \quad (3)$$

$$\mathbf{h}_i^{l+1} = \phi_h(\mathbf{h}_i^l, \mathbf{m}_i), \quad (4)$$

where ϕ_e is an edge function that computes a message embedding from node features, squared distance, and optional edge attributes a_{ij} . ϕ_x outputs a scalar weight for coordinate updates, based on \mathbf{m}_{ij} . ϕ_h is a node update function. C is a normalization constant, typically $C = 1/(|\mathcal{V}| - 1)$.

Eq. (2) ensures that the coordinate update is equivariant to rotations and translations by acting as a learnable radial vector field. EGNN combines geometric awareness with standard message passing, making it a powerful architecture for modeling 3D protein structures.

SE(3) Transformer. The SE(3) Transformer [17] is a neural architecture designed to model geometric data such as molecules and point clouds while respecting SE(3) symmetries, i.e., 3D rotations and translations. It achieves this through the integration of *Tensor Field Networks (TFNs)* [60] for equivariant message passing and *invariant attention mechanisms* for weighted aggregation. This section presents a unified formulation of the SE(3) Transformer, encompassing both TFN convolution and attention-based update steps.

Formally, each node i in the graph is associated with a position $\mathbf{x}_i \in \mathbb{R}^3$ and a set of typed features $\mathbf{f}_i = \bigoplus_{\ell \geq 0} \mathbf{f}_i^\ell$, where $\mathbf{f}_i^\ell \in \mathbb{R}^{(2\ell+1) \times d}$ denotes a rank- ℓ feature tensor (type- ℓ representation of $\text{SO}(3)$) with d channels.

The output features at node i and type ℓ are computed as:

$$\mathbf{f}_{\text{out},i}^\ell = \mathbf{W}_{\text{self}}^{\ell\ell} \mathbf{f}_{\text{in},i}^\ell + \sum_{k \geq 0} \sum_{j \in \mathcal{N}_i \setminus \{i\}} \alpha_{ij} \mathbf{W}^{\ell k}(\mathbf{x}_j - \mathbf{x}_i) \mathbf{f}_{\text{in},j}^k. \quad (1)$$

The first term is a type-preserving self-interaction, and the second term aggregates messages from neighbors $j \in \mathcal{N}_i$ via a convolution-like operation using TFN kernels $\mathbf{W}^{\ell k}(\mathbf{x}_j - \mathbf{x}_i)$, modulated by scalar attention weights $\alpha_{ij} \in \mathbb{R}$.

The kernel $\mathbf{W}^{\ell k} : \mathbb{R}^3 \rightarrow \mathbb{R}^{(2\ell+1) \times (2k+1)}$ is constructed to ensure SE(3)-equivariance, and is defined as a linear combination of spherical harmonic projections:

$$\mathbf{W}^{\ell k}(\mathbf{x}) = \sum_{J=|\ell-k|}^{\ell+k} \varphi_J^{\ell k}(\|\mathbf{x}\|) \sum_{m=-J}^J Y_{Jm}(\widehat{\mathbf{x}}) \mathbf{Q}_{Jm}^{\ell k}, \quad (2)$$

where $\widehat{\mathbf{x}} = \mathbf{x}/\|\mathbf{x}\|$, Y_{Jm} is the m -th spherical harmonic of order J , $\varphi_J^{\ell k}$ is a learnable radial function, and $\mathbf{Q}_{Jm}^{\ell k}$ are learnable matrices formed from Clebsch–Gordan coefficients. This construction guarantees equivariance under SE(3) transformations by disentangling radial and angular dependencies.

The attention weights α_{ij} are designed to be SE(3)-invariant and are computed via a dot-product attention mechanism:

$$\alpha_{ij} = \frac{\exp(\langle \mathbf{q}_i, \mathbf{k}_{ij} \rangle)}{\sum_{j' \in \mathcal{N}_i \setminus \{i\}} \exp(\langle \mathbf{q}_i, \mathbf{k}_{ij'} \rangle)}, \quad (3)$$

where the query vector \mathbf{q}_i and key vector \mathbf{k}_{ij} are both constructed from the input features through learned TFN mappings:

$$\mathbf{q}_i = \bigoplus_{\ell \geq 0} \sum_{k \geq 0} \mathbf{W}_Q^{\ell k} \mathbf{f}_{\text{in},i}^k, \quad \mathbf{k}_{ij} = \bigoplus_{\ell \geq 0} \sum_{k \geq 0} \mathbf{W}_K^{\ell k}(\mathbf{x}_j - \mathbf{x}_i) \mathbf{f}_{\text{in},j}^k. \quad (4)$$

Here, $\mathbf{W}_Q^{\ell k}$ and $\mathbf{W}_K^{\ell k}$ are TFN-type filters that output representations in the same basis, ensuring that the dot product is invariant under common $\text{SO}(3)$ actions.

Equivariance is preserved in the message-passing path through the linear combination of TFN kernels. The attention mechanism maintains invariance because it operates entirely in scalar (dot-product) space between representations of the same type, which are invariant under group actions due to orthonormality properties of spherical harmonics.

GVP. The Geometric Vector Perceptron (GVP) [27] is a neural module designed for learning over geometric data, in which each entity (e.g., an amino acid residue or atom) is represented by both scalar and vector features. Formally, given a pair (\mathbf{s}, \mathbf{V}) where $\mathbf{s} \in \mathbb{R}^n$ denotes scalar features and $\mathbf{V} \in \mathbb{R}^{n \times 3}$ denotes geometric vector features, the GVP outputs a new pair $(\mathbf{s}', \mathbf{V}') \in \mathbb{R}^m \times \mathbb{R}^{m \times 3}$. This transformation is designed to ensure that the scalar outputs remain invariant while the vector outputs are equivariant with respect to rotations and reflections in \mathbb{R}^3 .

The GVP proceeds via the following algorithm:

Algorithm 1 Geometric Vector Perceptron (GVP)

Input: Scalar features $\mathbf{s} \in \mathbb{R}^n$, vector features $\mathbf{V} \in \mathbb{R}^{n \times 3}$

Output: Updated features $(\mathbf{s}', \mathbf{V}') \in \mathbb{R}^m \times \mathbb{R}^{m \times 3}$

- 1: $\mathbf{V}_h \leftarrow \mathbf{W}_h \mathbf{V}$
 - 2: $\mathbf{V}_\mu \leftarrow \mathbf{W}_\mu \mathbf{V}_h$
 - 3: $\mathbf{s}_h \leftarrow \|\mathbf{V}_h\|_2$ (row-wise)
 - 4: $\mathbf{v}_\mu \leftarrow \|\mathbf{V}_\mu\|_2$ (row-wise)
 - 5: $\mathbf{s}_{h+n} \leftarrow \text{concat}(\mathbf{s}_h, \mathbf{s})$
 - 6: $\mathbf{s}_m \leftarrow \mathbf{W}_m \mathbf{s}_{h+n} + \mathbf{b}$
 - 7: $\mathbf{s}' \leftarrow \sigma(\mathbf{s}_m)$
 - 8: $\mathbf{V}' \leftarrow \sigma_+(\mathbf{v}_\mu) \odot \mathbf{V}_\mu$ **return** $(\mathbf{s}', \mathbf{V}')$
-

Here, \mathbf{W}_h , \mathbf{W}_μ , and \mathbf{W}_m are learnable linear transformations, while σ and σ_+ are nonlinear activation functions (e.g., ReLU, GELU, or their variants). The vector norm computations $\|\cdot\|_2$ are row-wise and used to extract invariant scalar information from the geometric vectors, which is then injected into the scalar pathway before transformation. The final output \mathbf{V}' is modulated via element-wise multiplication with a positive gating function $\sigma_+(\mathbf{v}_\mu)$ to preserve equivariance.

The GVP-GNN updates node embeddings $h_v^{(i)}$ via message passing:

$$h_m^{(j \rightarrow i)} = \text{GVP} \left(\text{concat}(h_v^{(j)}, h_e^{(j \rightarrow i)}) \right), \quad (1)$$

$$h_v^{(i)} \leftarrow \text{LayerNorm} \left(h_v^{(i)} + \frac{1}{k'} \sum_{j \in \mathcal{N}_i} \text{Dropout}(h_m^{(j \rightarrow i)}) \right), \quad (2)$$

Here, $\text{GVP}(\cdot)$ denotes a sequence of three GVPs. The embeddings $h_v^{(i)}$ and $h_e^{(j \rightarrow i)}$ correspond to node i and edge $(j \rightarrow i)$, respectively, as previously defined. The message $h_m^{(j \rightarrow i)}$ is computed from these embeddings and represents the information passed from node j to node i . The variable k' denotes the number of incoming messages, which equals k unless the protein contains fewer than k amino acid residues. Then, a feed-forward point-wise layer is utilized to update the node embeddings at all nodes i :

$$h_v^{(i)} \leftarrow \text{LayerNorm} \left(h_v^{(i)} + \text{Dropout}(\text{GVP}(h_v^{(i)})) \right), \quad (3)$$

where $\text{GVP}(\cdot)$ is a sequence of two GVPs. This architecture allows for expressive, symmetry-aware modeling of protein geometry with built-in equivariance, while remaining efficient and conceptually simple.

ProteinBERT. ProteinBERT [6] is a denoising autoencoder for proteins, inspired by BERT [13] but with a distinct architecture.

It takes two inputs: amino acid sequences and GO annotations. The architecture consists of parallel local and global pathways. Local representations are 3D tensors of shape $B \times L \times d_{\text{local}}$ (with $d_{\text{local}} = 128$), and global representations are 2D tensors of shape $B \times d_{\text{global}}$ (with $d_{\text{global}} = 512$).

Each input sequence is embedded into local features by a shared position-wise embedding layer, while annotations are mapped into global features via a fully connected layer. The model applies six transformer-like blocks [63], each updating local features using both narrow and dilated convolutions (kernel size 9, dilation 1 and 5), followed by feedforward layers. The global path consists of two fully connected layers per block.

Local-global interaction occurs via (1) a broadcast fully connected layer from global to local, and (2) a global attention layer from local to global. Global attention has linear complexity and uses trainable projection matrices W_q , W_k , and W_v (with $d_{\text{key}} = 64$, $d_{\text{value}} = 128$), and $n_{\text{heads}} = 4$ per block. All activations use GELU [22].

D-Transformer. D-Transformer augments the Transformer with 3D knowledge by adding pairwise $C\alpha$ distances to the self-attention scores, similar to Transformer-M [36]. For a protein of length L , let $\mathbf{X} = [\mathbf{x}_1, \dots, \mathbf{x}_L] \in \mathbb{R}^{L \times d}$ be residue embeddings and $D(i, j) = \|\mathbf{r}_i - \mathbf{r}_j\|_2$ the Euclidean distance between residues i and j .

Each distance is first expanded with a learnable Gaussian radial basis:

$$\phi_{\text{dist}}(D(i, j)) = \left[\exp\left(-\frac{(D(i, j) - \mu_k)^2}{2\sigma_k^2}\right) \right]_{k=1}^K, \quad (1)$$

where $\{\mu_k, \sigma_k\}_{k=1}^K$ are trainable parameters. A multilayer perceptron maps this K -vector to a scalar bias $b_{ij} = \text{MLP}(\phi_{\text{dist}}(D(i, j)))$.

For one attention head, the unnormalised score is

$$A_{ij} = \frac{(\mathbf{h}_i W_Q)(\mathbf{h}_j W_K)^T}{\sqrt{d}} + b_{ij}, \quad (2)$$

with \mathbf{h}_i the hidden state at residue i and learned $W_Q, W_K \in \mathbb{R}^{d \times d}$. Because b_{ij} depends only on distances, A_{ij} is invariant to global rotations, translations, and residue permutations. Normalised weights and value aggregation follow standard Transformer rules:

$$\alpha_{ij} = \text{softmax}_j(A_{ij}), \quad \mathbf{z}_i = \sum_{j=1}^L \alpha_{ij} (\mathbf{h}_j W_V), \quad (3)$$

where $W_V \in \mathbb{R}^{d \times d}$. A position-wise feed-forward network with residual connections completes each layer, and stacking multiple such layers yields a lightweight architecture that leverages structural information without coordinate updates.

ESM2. ESM-2 [35] is a family of transformer-based protein language models trained to predict masked amino acids in protein sequences. Compared to its predecessor ESM-1b [54], ESM-2 introduces architectural refinements, improved training procedures, and is scaled across model sizes ranging from 8M to 15B parameters. The model is trained using a standard masked language modeling (MLM) objective: for 15% randomly masked positions in a sequence, the model predicts the identity of each masked amino acid based on its unmasked context.

Formally, the training objective is:

$$\mathcal{L}_{\text{MLM}} = \sum_{i \in \mathcal{M}} \log p(x_i | x_{\setminus \mathcal{M}}), \quad (1)$$

where M is the set of masked positions and $x_{\setminus M}$ denotes the observed amino acids. Training is performed on ~ 65 million sequences sampled from ~ 43 million UniRef50 [10] clusters, covering ~ 138 million UniRef90 entries.

Despite its unsupervised formulation, ESM-2 learns rich structural features purely from sequence data. The model achieves state-of-the-art performance on several protein structure prediction benchmarks and surpasses previous models, e.g., ESM-1b, ProteinBERT.

G.2 Pretrain Model Experimental Setup

In this section, we provide more details about the pertaining.

Table 16: Hyperparameter setting of the EGNN pre-training.

MLM	
Batch Size	48
Learning Rate	1e-3
Warmup Ratio	0.05
Mask Ratio	0.15
Hidden Dimension	512
Layer Depth	3
MVCL	
Batch Size	96
Learning Rate	1e-3
Warmup Ratio	0.05
Subsequence Length	50
Max Node	50
Temperature	0.0099
Hidden Dimension	512
Layer Depth	3
PFP	
Batch Size	48
Learning Rate	1e-3
Warmup Ratio	0.05
Temperature	0.01
Hidden Dimension	512
Layer Depth	3

Pre-training Data. The structural information used for pretraining is derived from the AFDB Swiss-Prot dataset, while the functional and family annotations are obtained from UniProt Swiss-Prot. Swiss-Prot is a high-quality, manually curated protein sequence database within UniProt. Its goal is to provide comprehensive and biologically meaningful annotations of protein sequences, such as their functions, families, and maintain minimal redundancy. The AFDB Swiss-Prot dataset is a subset of the AlphaFold Protein Structure Database that specifically contains structure predictions for all protein sequences corresponding to UniProt Swiss-Prot entries. Currently, the dataset includes a total of 542,378 entries. ESM-2 and SaProt are pretrained on UniRef sequences clustered at the 50% sequence identity level. ESM-C is also pretrained on UniRef but with clustering at the 70% sequence identity level, and further incorporates protein sequences from the MGnify and Joint Genome Institute (JGI) databases, resulting in 83M, 372M, and 2B clusters for UniRef, MGnify, and JGI, respectively.

Table 17: Hyperparameter setting of the SE(3) Transformer pre-training.

MLM	
Batch Size	48
Learning Rate	1e-2
Warmup Ratio	0.05
Mask Ratio	0.15
Hidden Dimension	36
Layer Depth	2
MVCL	
Batch Size	96
Learning Rate	1e-2
Warmup Ratio	0.05
Subsequence Length	50
Max Node	50
Temperature	0.0099
Hidden Dimension	36
Layer Depth	2
PFP	
Batch Size	48
Learning Rate	1e-3
Warmup Ratio	0.05
Temperature	0.0099
Hidden Dimension	36
Layer Number	2

Settings. We adopt task and architecture-specific training and model hyperparameters across different pretraining tasks and model types. Detailed configurations are summarized in Tab. 16-20.

For the Multi-View Contrastive Learning (MVCL) task, we set the maximum length of sub-sequences to 50. To extract substructures in 3D space, we randomly sample a central amino acid and collect all residues within a 15 Å Euclidean radius, with the subspace length capped at 50 residues. Temperature values used in the contrastive objective are adapted for each model architecture to ensure stable training dynamics.

For the Protein Family Prediction (PFP) task, we address the sparsity of family labels by adopting a negative sampling strategy. During training, family labels are embedded into the same representation space as proteins, and the model is optimized to align protein embeddings with their corresponding family embeddings. Simultaneously, embeddings of proteins from other families within the same batch are pushed apart, following a contrastive learning framework. A temperature coefficient is introduced to scale the similarity scores and enhance training stability.

H Domain-Specific Model Architecture

KDBNet. KDBNet [37] is a graph neural network model designed for predicting kinase–small molecule binding affinity. It constructs heterogeneous graph pairs from the 3D structures of protein binding pockets and small molecules, and employs two structure-aware GNNs to learn their respective representations. For the protein, the model focuses on 85 binding site residues defined by the KLIFS

Table 18: Hyperparameter setting of the D-Transformer pre-training.

MLM	
Batch Size	16
Learning Rate	1e-4
Warmup Ratio	0.1
Mask Ratio	0.15
Hidden Dimension	256
Layer Depth	6
MVCL	
Batch Size	16
Learning Rate	1e-4
Warmup Ratio	0.1
Subsequence Length	50
Max Node	50
Temperature	0.01
Hidden Dimension	256
Layer Depth	6
PFP	
Batch Size	16
Learning Rate	1e-4
Warmup Ratio	0.1
Temperature	0.01
Hidden Dimension	256
Layer Number	6

Table 19: Hyperparameter setting of the GVP pre-training.

MLM	
Batch Size	64
Learning Rate	1e-4
Warmup Ratio	0.1
Mask Ratio	0.15
Node Dimension	(155,16)
Layer Depth	3
MVCL	
Batch Size	64
Learning Rate	1e-4
Warmup Ratio	0.1
Subsequence Length	50
Max Node	50
Temperature	0.01
Node Dimension	(155,16)
Layer Depth	3
PFP	
Batch Size	64
Learning Rate	1e-4
Warmup Ratio	0.1
Temperature	0.01
Node Dimension	(155,16)
Layer Number	3

Table 20: Hyperparameter setting of the ProteinBERT pre-training.

MLM	
Batch Size	48
Learning Rate	1e-4
Warmup Ratio	0.05
Mask Ratio	0.15
Hidden Dimension	512
Layer Depth	12
MVCL	
Batch Size	96
Learning Rate	1e-4
Warmup Ratio	0.05
Subsequence Length	50
Max Node	50
Temperature	0.0099
Hidden Dimension	512
Layer Depth	12
PFP	
Batch Size	48
Learning Rate	1e-4
Warmup Ratio	0.05
Temperature	0.0099
Hidden Dimension	512
Layer Depth	12

database to build a structure graph $\mathcal{G}_p = (\mathcal{V} * p, \mathcal{E} * p)$, where nodes represent residues and edges are formed between C* α atoms within 8 Å. Each residue node includes three types of features: one-hot encoding of amino acid type, geometric features based on backbone conformation (e.g., $(\sin \phi_i, \sin \psi_i, \sin \omega_i, \cos \phi_i, \cos \psi_i, \cos \omega_i)$), and evolutionary embeddings obtained from the ESM language model. Edge features consist of four components: radial basis function (RBF) encoding of distances, local frame-based projections of relative direction vectors, rotational quaternions between residues, and relative position encodings using a Transformer-based function $E * \text{pos}(c_j - c_i)$. The small molecule is represented as a graph $\mathcal{G}_d = (\mathcal{V}_d, \mathcal{E}_d)$, where atoms are nodes and edges connect atom pairs within 4.5 Å. Each atom node includes both 3D coordinates and a 66-dimensional scalar feature vector describing chemical properties, while edge features include unit directional vectors and RBF-encoded distances. For encoding protein structure, KDBNet uses a Graph Transformer, where each layer updates node features via the following attention mechanism:

$$h_i^{(\ell)} = W_1^{(\ell)} h_i^{(\ell-1)} + \sum_{j \in \mathcal{N}(i)} \alpha_{ij} \left(W_2^{(\ell)} h_j^{(\ell-1)} + W_3^{(\ell)} e_{ij} \right). \quad (1)$$

With attention weights defined as:

$$\alpha_{ij} = \text{softmax} \left(\frac{\left(W_4^{(\ell)} h_i^{(\ell-1)} \right)^\top \left(W_5^{(\ell)} h_j^{(\ell-1)} + W_3^{(\ell)} e_{ij} \right)}{\sqrt{d_\ell}} \right). \quad (2)$$

Three such graph convolution layers are stacked with Leaky ReLU activations, and global sum pooling is applied to obtain the final protein embedding. For small molecules, KDBNet adopts the GVP-GNN architecture, which jointly models vector and scalar features to maintain rotational and translational equivariance. Each atom node is represented as a tuple (v_i^v, v_i^s) and each edge as (e_{ij}^v, e_{ij}^s) , where the vector part allows direct alignment with atomic coordinates. The final protein and drug embeddings are passed through fully connected layers to regress the binding affinity.

DeepPROTACs. DeepPROTAC [32] is a deep learning framework designed to predict the degradation efficacy of PROTAC molecules by integrating structural and chemical information from multiple components: the protein of interest (POI), the E3 ligase, and the PROTAC compound itself. The input includes five parts: the POI binding pocket, the E3 ligase binding pocket, the warhead (the PROTAC moiety binding to the POI), the E3 ligand (binding to the E3 ligase), and the linker represented as a SMILES string. For the four molecular structures (POI pocket, E3 pocket, warhead, and E3 ligand), atom-level graphs are constructed and processed using Graph Convolutional Layers (GCLs) followed by max pooling to obtain fixed-size feature embeddings. The linker is embedded using an LSTM network to capture sequential chemical features. All five embeddings are concatenated and passed through fully connected layers to yield a binary output: 1 indicates good degradation (defined as $DC_{50} \leq 100$ nM and $D_{max} \geq 80\%$), while 0 indicates poor degradation ($DC_{50} > 100$ nM or $D_{max} < 80\%$). This modular architecture enables DeepPROTACs to effectively model ternary complex formation and predict degradation outcomes based on both structural and sequential representations.

ET-PROTACs. ET-PROTACs [8] is an end-to-end deep learning model designed for PROTAC degradation prediction, consisting of four main components: (i) initial PROTAC and protein featurization; (ii) representation learning using 3D graph-based and sequence-based encoders; (iii) a cross-modal ternary attention block; and (iv) a final classifier. Each component is described in detail below. Each PROTAC is represented as a 2D molecular graph $\mathcal{G} = (\mathcal{V}, \mathcal{E})$ and associated with a 3D coordinate matrix $X \in \mathbb{R}^{|\mathcal{V}| \times 3}$ using RDKit¹. Nodes $v_i \in \mathcal{V}$ represent atoms, and edges $a_{ij} \in \mathcal{E}$ denote chemical bonds. Node features h_i and edge features a_{ij} are encoded using learned embeddings. Additionally, atomic 3D coordinates $x_i \in \mathbb{R}^3$ are embedded to capture spatial information. The input protein is given as a sequence $P = \{a_1, a_2, \dots, a_n\}$ of 23 amino acids (including one non-standard residue). Protein sequences are encoded by two embedding layers: a learned character embedding of dimension 64, and a positional embedding of the same dimension. The molecular graph and 3D coordinates are processed by an Equivariant Graph Neural Network (EGNN), which is invariant to rotations and translations. Let h_i^ℓ , x_i^ℓ , and a_{ij} be the node features, coordinates, and edge features at layer ℓ , respectively. The EGNN updates are as follows:

$$\begin{aligned} m_{ij} &= \phi_e(h_i^\ell, h_j^\ell, \|x_i^\ell - x_j^\ell\|^2, a_{ij}), \\ x_i^{\ell+1} &= x_i^\ell + C \sum_{j \neq i} (x_i^\ell - x_j^\ell) \phi_x(m_{ij}), \\ m_i &= \sum_{j \in \mathcal{N}(i)} m_{ij}, \\ h_i^{\ell+1} &= \phi_h(h_i^\ell, m_i), \end{aligned} \quad (1)$$

where $C = 1/(M - 1)$, ϕ_e , ϕ_x , and ϕ_h are learnable functions, and M is the number of atoms. Final PROTAC embeddings are obtained by combining features of the warhead, linker, and E3 ligase substructures. ET-PROTACs leverages CNNs to encode protein sequences directly from FASTA format. The sequence embedding E is passed through three CNN layers to yield latent protein features $P_{\text{cnn}} \in \mathbb{R}^{d \times f}$, where f is the number of filters in the last layer. Given feature matrices $D = \{d_1, \dots, d_X\}$ (PROTAC), $P = \{p_1, \dots, p_Y\}$ (protein), and $L = \{l_1, \dots, l_Z\}$ (ligase), we form composite pairs:

$$\begin{aligned} \text{pd}_i &= \text{CONCAT}(p_j, d_i), \\ \text{dl}_j &= \text{CONCAT}(d_i, l_k), \\ \text{pda}_i &= F(W_{\text{pd}} \cdot \text{pd}_i + b), \\ \text{dla}_j &= F(W_{\text{dl}} \cdot \text{dl}_j + b), \end{aligned} \quad (2)$$

where F is a non-linear activation, and $W_{\text{pd}}, W_{\text{dl}} \in \mathbb{R}^{f \times f}$ are learned weights. The combined attention is computed as:

$$\begin{aligned} A_{i,j} &= F(W_a \cdot (\text{pda}_i + \text{dla}_j) + b), \\ A_{\text{pd}} &= \sigma(\text{MEAN}(A, 2)), \\ A_{\text{dl}} &= \sigma(\text{MEAN}(A, 1)), \end{aligned} \quad (3)$$

where σ denotes the sigmoid function. The resulting outputs V_{pd} and V_{dl} are the attention-enriched representations of PROTAC-protein and PROTAC-ligase interactions. The attention outputs are pooled over sequence length and concatenated:

$$s = \text{LeakyReLU}(W_s \cdot \text{CONCAT}(V_{\text{pd}}, V_{\text{dl}}) + b_s), \quad (4)$$

where W_s is a learnable weight matrix. Dropout is applied before and after each linear layer to prevent overfitting.

DeepFRI. DeepFRI [20] is a deep learning framework for protein function prediction based solely on amino acid sequences. Given a protein sequence of length L , the input is encoded as a binary matrix $X = [x_1, \dots, x_L] \in \{0, 1\}^{L \times 26}$, where each x_i is a one-hot vector indicating the amino acid type at position i , including 20 standard residues, 5 non-standard residues, and a gap symbol. This input is passed through a set of one-dimensional convolutional layers, each consisting of $f_n = 512$ filters of varying kernel lengths f_i , followed by rectified linear unit (ReLU) activation, $\text{ReLU}(x) = \max(x, 0)$, and a global max-pooling operation. The use of multiple filter sizes enables the extraction of complementary local patterns from the sequence. Outputs from 16 such CNN layers are concatenated, resulting in an $L \times 8192$ feature representation. Finally, a fully connected layer with sigmoid activation outputs probabilities for either Gene Ontology (GO) terms or Enzyme Commission (EC) classes. The output dimensionality is task-specific, corresponding to $|\text{GO}|$ or $|\text{EC}|$ respectively.

DPFunc. DPFunc [64] is a structure-aware protein function prediction framework that captures residue-level information by integrating 3D geometric structure and pretrained sequence embeddings.

¹<https://www.rdkit.org/>

For a given protein of length l , a residue-level undirected graph is constructed where each node represents a residue, and an edge is added between two residues if the distance between their C_α atoms is less than 10 Å. This defines the adjacency matrix $A \in \{0, 1\}^{l \times l}$. Node features are initialized using embeddings from a pretrained protein language model (ESM-1b), resulting in $X \in \mathbb{R}^{l \times d}$. Two graph convolutional layers are then used to propagate structural information, with residual connections added to facilitate gradient flow. The update rule for the k -th GCN layer is given by:

$$X^{(k+1)} = X^{(k)} + \text{ReLU}(\tilde{D}^{-1/2} \tilde{A} \tilde{D}^{-1/2} X^{(k)} W^{(k)}), \quad (1)$$

where $\tilde{A} = A + I$ adds self-loops and \tilde{D} is its corresponding degree matrix. After GCN propagation, domain-level information is introduced to enhance residue representations. Protein domains are annotated using InterProScan, and their one-hot encoding $IPR \in \{0, 1\}^{1 \times m}$ is mapped to dense embeddings via two fully connected layers with ReLU activations:

$$H = \text{ReLU}((\text{ReLU}(IPR \cdot W_{\text{emd}}) W_1 + b_1) W_2 + b_2). \quad (2)$$

A domain-guided attention mechanism, inspired by the Transformer encoder, is applied to model the interaction between domain and residue representations. For each attention head i , the query, key, and value matrices are computed as:

$$Q_i = H W_i^Q, \quad K_i = X_{\text{final}} W_i^K, \quad V_i = X_{\text{final}} W_i^V, \quad (3)$$

and attention weights are derived as:

$$W_i^A = \text{Softmax}\left(\frac{K_i Q_i^T}{\sqrt{d}}\right). \quad (4)$$

The multi-head attention output is computed as:

$$X_{\text{multi}} = \text{LayerNorm}\left(\text{Concat}(W_1^A V_1, \dots, W_n^A V_n) W_{\text{trans}} + X_{\text{final}}\right), \quad (4)$$

followed by a feedforward transformation with residual connection:

$$X_{\text{out}} = \text{LayerNorm}(\text{FF}(X_{\text{multi}}) + X_{\text{multi}}). \quad (5)$$

Protein-level features are then obtained by summing across residues:

$$x_{\text{pool}} = \sum_{i=1}^l X_{\text{out}}[i]. \quad (6)$$

This representation is concatenated with the average of initial residue features:

$$x_{\text{integrate}} = \text{Concat}\left(x_{\text{pool}}, \frac{1}{l} \sum_{i=1}^l X[i]\right), \quad (7)$$

and passed through a multilayer perceptron with sigmoid activation to produce GO term probabilities:

$$\hat{y} = \text{Sigmoid}(\text{MLP}(x_{\text{integrate}})). \quad (8)$$

To ensure consistency with the GO hierarchy, a postprocessing step enforces that if a child term is predicted, all its ancestors are also predicted:

$$\hat{y}_i^{\text{post}} = \max(\hat{y}_i, \hat{y}_{\text{child}_1}, \dots, \hat{y}_{\text{child}_n}). \quad (9)$$

This hierarchical correction is applied only after inference, without affecting training efficiency.

UniZyme. UniZyme [31] is a biochemically informed framework designed to generalize protein cleavage site prediction across diverse enzymes. It comprises an enzyme encoder and a substrate encoder. The enzyme encoder integrates sequence-derived features with energetic frustration and 3D structural information. Given an enzyme $P_e = (X, R)$, where X are residue embeddings and R are C^α coordinates, the pairwise frustration score is defined as:

$$F(i, j) = \frac{E(i, j) - \mu_{\text{rand}}(i, j)}{\sigma_{\text{rand}}(i, j)}. \quad (1)$$

To incorporate spatial and energetic cues into the self-attention mechanism, each residue pair is encoded via Gaussian basis kernels:

$$\Phi_{i,j}^{\text{energy}} = \text{MLP}(\phi_{\text{energy}}(F(i, j))), \quad \Phi_{i,j}^{\text{dist}} = \text{MLP}(\phi_{\text{dist}}(\|r_i - r_j\|_2)). \quad (2)$$

These terms are added to the attention score matrix in the graph transformer:

$$A_{i,j}^k = \frac{(h_i^{k-1} W_Q)(h_j^{k-1} W_K)^T}{\sqrt{d}} + \Phi_{i,j}^{\text{energy}} + \Phi_{i,j}^{\text{dist}}. \quad (3)$$

To guide the encoder toward catalytically relevant regions, an auxiliary active-site prediction is introduced:

$$\hat{a}_i = \sigma(h_i \cdot w_a). \quad (4)$$

The predicted probabilities \hat{a}_i are then used in a soft attention-like pooling mechanism for enzyme representation:

$$h_e = \sum_{i=1}^N \frac{f(\hat{a}_i)}{\sum_j f(\hat{a}_j)} h_i. \quad (5)$$

For a substrate P_s , cleavage site prediction is formulated by concatenating local substrate representations $H_s^{t:t+l}$ with the enzyme representation h_e :

$$\hat{c}_{e,s}^{(t)} = \text{MLP}(\text{CONCAT}(H_s^{t:t+l}, h_e)). \quad (6)$$

The model is jointly optimized using binary cross-entropy losses for both tasks:

$$\mathcal{L} = \mathcal{L}_c(D_c) + \lambda \mathcal{L}_a(D_a). \quad (7)$$

MONN. MONN [34] is composed of four interconnected modules: a graph convolutional module for molecular representation, a CNN module for residue-level protein representation, a pairwise interaction module for atom-residue interaction estimation, and an affinity prediction module for compound-protein binding affinity estimation.

Given a molecular graph $G = (V, E)$, each atom $v_i \in V$ is initially represented by an 82-dimensional one-hot vector v_i^{init} encoding atomic features. These are projected into a hidden space \mathbb{R}^{h_1} by:

$$v_i^0 = f(W_{\text{init}} v_i^{\text{init}}), \quad (1)$$

where $f(x) = \max(0, x) + 0.1 \min(0, x)$ is the leaky ReLU activation, and $W_{\text{init}} \in \mathbb{R}^{h_1 \times 82}$. Bonds $e_{i,j} \in E$ are represented by 6-dimensional one-hot vectors encoding bond type and topology.

For L graph convolutional iterations, features are updated by message passing and graph warp. At each layer l , local messages are aggregated:

$$t_i^l = \sum_{v_k \in \mathcal{N}(v_i)} f(W_{\text{gather}}^l [v_k^{l-1}, e_{i,k}]), \quad (2)$$

followed by feature updates:

$$u_i^l = f(W_{\text{update}}^l [t_i^l, v_i^{l-1}]). \quad (3)$$

Global information is captured via a super node s^l that interacts with all u_i^l to yield the final atom features $\{v_i^l\}$ and compound feature s^l .

Protein sequences are encoded by mapping residues to BLOSUM62 [14] columns and processed through a 1D CNN to obtain residue embeddings $\{r_j\}$ in \mathbb{R}^{h_1} .

Atom-residue interactions are predicted by projecting atom and residue embeddings to a shared space and computing their dot-product, followed by a sigmoid:

$$P_{i,j} = \sigma(f(W_{\text{atom}} v_i) \cdot f(W_{\text{residue}} r_j)). \quad (4)$$

For affinity prediction, atom, residue, and super node features are transformed via:

$$h_{v,i} = f(W_v v_i), \quad h_s = f(W_s s), \quad h_{r,j} = f(W_r r_j), \quad (5)$$

where $W_v, W_r, W_s \in \mathbb{R}^{h_2 \times h_1}$. A modified dual attention network uses the interaction matrix P to compute attentions $\{\alpha_{v,i}\}, \{\alpha_{r,j}\}$, aggregating compound and protein representations as:

$$h_c = \sum_i \alpha_{v,i} h_{v,i}, \quad h_p = \sum_j \alpha_{r,j} h_{r,j}. \quad (6)$$

The binding affinity is predicted by a regression on the outer product between $[h_c, h_s]$ and h_p :

$$a = W_{\text{affinity}} f(\text{flatten}([h_c, h_s] \otimes h_p)), \quad (7)$$

where $W_{\text{affinity}} \in \mathbb{R}^{1 \times 2h_2^2}$.

CLIPZyme. CLIPZyme [41] formulates enzyme screening as a retrieval task, where a predefined set of enzymes is ranked based on their predicted ability to catalyze a given chemical reaction. Each reaction R and enzyme P is encoded into a d -dimensional vector $r, p \in \mathbb{R}^d$ using learned encoders f_{rxn} and f_p , respectively. A scoring function $s(r, p)$ computes the cosine similarity between the two embeddings:

$$s_{ij} = s(r_i, p_j) = \frac{r_i \cdot p_j}{\|r_i\| \|p_j\|}. \quad (1)$$

To align reactions with their catalyzing enzymes, a symmetric contrastive loss is used:

$$\mathcal{L}_{ij} = -\frac{1}{2N} \left(\log \frac{e^{s_{ij}/\tau}}{\sum_k e^{s_{ik}/\tau}} + \log \frac{e^{s_{ij}/\tau}}{\sum_k e^{s_{kj}/\tau}} \right), \quad (2)$$

where τ is a temperature parameter and negative samples are drawn from other enzymes in the batch.

To represent a reaction, atom-mapped molecular graphs of the reactants G_x and products G_y are first encoded by a directed message passing neural network [69] (DMPNN) f_{mol} , yielding atom features a_i and bond features b_{ij} :

$$a_i, b_{ij} = f_{\text{mol}}(G_x, G_y). \quad (3)$$

A pseudo-transition state graph G_{TS} is then constructed using shared atom features and summed bond features:

$$v_i^{(TS)} = v_i^{(x)} = v_i^{(y)}, \quad (3)$$

$$e_{ij}^{(TS)} = b_{ij}^{(x)} + b_{ij}^{(y)}. \quad (4)$$

This graph is processed by a second DMPNN f_{TS} , and the reaction embedding is obtained by aggregating the learned node features:

$$a'_i, b'_{ij} = f_{TS}(G_{TS}), \quad (4)$$

$$r = \sum_i a'_i. \quad (5)$$

Each protein is modeled as a 3D graph $G_p = (V, E)$ with node features h_i , edge features e_{ij} , and 3D coordinates $c_i \in \mathbb{R}^3$. Residue features are initialized using ESM-2 (650M) embeddings with dimensionality 1280. An EGNN with coordinate updates is used to encode G_p into the final protein embedding $p = f_p(G_p)$. Relative distances between residues are encoded using a sinusoidal basis to enhance structural modeling.